Front. Mech. Eng. 2020, 15(3): 438–474
https://doi.org/10.1007/s11465-019-0579-1

REVIEW ARTICLE

Vivek PATEL, Gaurav TIWARI, Ravikumar DUMPALA

Review of the crushing response of collapsible tubular structures

Abstract Studies on determining and analyzing the crushing response of tubular structures are of significant interest, primarily due to their relation to safety. Several aspects of tubular structures, such as geometry, material, configuration, and hybrid structure, have been used as criteria for evaluation. In this review, a comprehensive analysis of the important findings of extensive research on understanding the crushing response of thin-walled tubular structures is presented. Advancements in thin-walled structures, including multi-cell tube, honeycomb and foam-filled, multi wall, and functionally graded thickness tubes, are also discussed, focusing on their energy absorption ability. An extensive review of experimentation and numerical analysis used to extract the deformation behavior of materials, such as aluminum and steel, against static and dynamic loadings are also provided. Several tube shapes, such as tubes of uniform and nonuniform (tapered) cross sections of circular, square, and rectangular shapes, have been used in different studies to identify their efficacy. Apart from geometric and loading parameters, the effects of fabrication process, heat treatment, and triggering mechanism on initiating plastic deformation, such as cutouts and grooves, on the surface of tubular structures are discussed.

Keywords monolithic structure, crashworthiness, energy absorber, static and dynamic loadings, multicellular tube structure, filled tube

1 Introduction

With the advancement of combustion engines, the use of high-speed vehicles in daily life is increasing day by day. Safety requirements should be enhanced to mitigate probable accidental damages. The occurrence of impact or collision involving automobiles is a common phenomenon associated with their use. In this context, engineers and researchers are continuously attempting to develop structures that can absorb most of the energy transferred to a vehicle during collision, such that minimum or no damage can occur to the passengers. The capability of a structure to absorb impact energy in a stable manner and provide safety to its occupants is known as crashworthiness. The geometry and material of a structure are important aspects to consider when developing an efficient energy-absorbing component.

Numerous studies have been conducted on different structures, such as monolithic tubes with different cross sections, multi-tubular and corrugated tubes, sandwich structures with a honeycomb or foam core, and multi cell tubes. The performance of structures against crushing loads (longitudinal, oblique, and eccentric loading compression) has been evaluated in terms of peak force ($F_{\max}$), mean crushing force ($\overline{F}$), energy absorption capacity (E_{ab}), specific energy absorption (*SEA*), crash force efficiency (*CFE*), and stroke efficiency (*SE*), which are defined as follows [1]:

1) Peak force ($F_{\max}$)

The maximum initial load attained by a collapsible structure during an impact is known as peak force.

2) Mean crushing force ($\overline{F}$)

To clearly visualize impact load on the force–displacement graph with reference to the initial peak force, mean crushing force, which reflects the structure deformation pattern, should be plotted.

3) Crash force efficiency (*CFE*)

It is the ratio of the average or mean crushing load to the initial peak load. It should be high for a good absorber.

$$CFE = \frac{\overline{F}}{F_{\max}}. \tag{1}$$

Received May 31, 2019; accepted November 23, 2019

Vivek PATEL (✉), Gaurav TIWARI, Ravikumar DUMPALA
Department of Mechanical Engineering, Visvesvaraya National Institute of Technology, Nagpur 440010, India
E-mail: vivekmanit0031@gmail.com

4) Stroke efficiency (*SE*)

As a tube deforms, it shortens and forms many folds, by which force resistance increases. Therefore, *SE* is defined as the ratio of the crushed height (h) to the original height (L).

$$SE = \frac{h}{L}. \tag{2}$$

5) Energy absorption capacity (E_{ab})

It refers to the area under the force–displacement curve that exhibits the energy absorption capability of the structure. It is measured by integrating the load (F) with respect to the deformed or crushed height.

$$E_{ab} = \int_0^h F(h)\mathrm{d}h. \tag{3}$$

6) Specific energy absorption (*SEA*)

It is defined as the energy absorbed per unit mass of the crushed component.

$$SEA = \frac{E_{ab}}{m}. \tag{4}$$

All the aforementioned parameters are measured through the force versus displacement curve, as shown in Fig. 1.

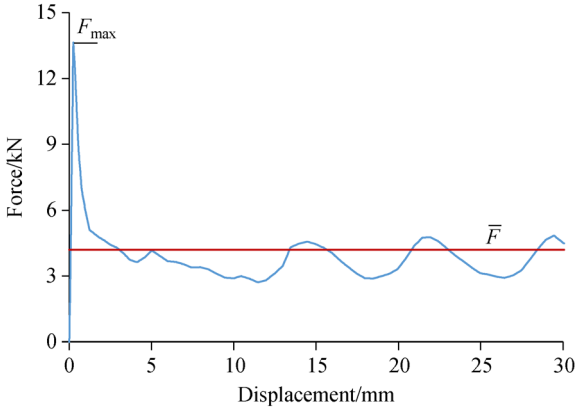

Fig. 1 Force vs. displacement curve of tubular structures used for measuring crashworthiness parameters.

This study summarizes the crushing response of thin-walled energy-absorbing structures that are mostly used in the automobile industry. Structures that collapsed via splitting or inversion deformation mode are beyond the scope of this study because these deformation modes are not frequently used in vehicle bodies [2]. The structures included in the present study are classified as shown in Fig. 2 based on the extensive survey of the literature that pertains to static and dynamic loading conditions.

This paper is structured in sections. Section 2 focuses on the methodologies adopted by different researchers based on experimental and numerical analyses. Section 3 discusses the different monolithic structures with loading condition and chosen material. Section 4 presents advancements in monolithic structures. Section 5 indicates the results and discussion. Section 6 provides guidance on future developments of the tubular structure. Section 7 provides the concluding remarks about the better crashworthiness functioning of the structures used as an energy-absorbing component.

2 General approaches

Researchers have studied the crashworthiness performance of tubular structures by adopting methodologies that help analyze the effects of different geometric parameters using experimental and simulation tests under quasi-static and dynamic loading conditions.

2.1 Experimental setup

The crashworthiness characteristics of tubular structures are examined through an experimental test under two different loading conditions: Quasi-static and dynamic. The quasi-static analysis approach is frequently used to design structures that are subject to dynamic loading. It helps simplify the analytical approach. Quasi-static analysis is conducted using a compression testing machine with a velocity within the range of 2–10 mm/min. A dynamic test evaluates the behavior of a structure against the actual condition of crashing that shows the unstable deformation modes due to the dominance inertia effect. Impactor mass and its velocity, which control the impact energy subjected on the structure, are of primary consideration to perform the dynamic test.

2.2 Numerical simulation setup

For numerical simulations, different finite element analysis codes, such as ABAQUS, ANSYS (e.g., AUTODYNE and LS-DYNA) and COMSOL, are available. The crushing phenomenon has been simulated by placing the target structure in between two rigid plates. The Belytschko–Tsay shell element has been considered by most researchers to model tubular structures. The structure in this study comprises a nonlinear property of a selected collapsible material, and fixed and moving plates are considered a rigid body. Contact between the rigid surface (both plates, i.e., movable and fixed plates) and the tube structure is provided as an automatic surface-to-surface contact. For a large deformation case under quasi-static loading, simulation time can be reduced by adopting some techniques mentioned in LS-DYNA user's manual [3], which are as follows:

- Loading rate should be increased, with the inertia and strain rate effects being disregarded.
- Mass scaling is adopted for a stable time step size.

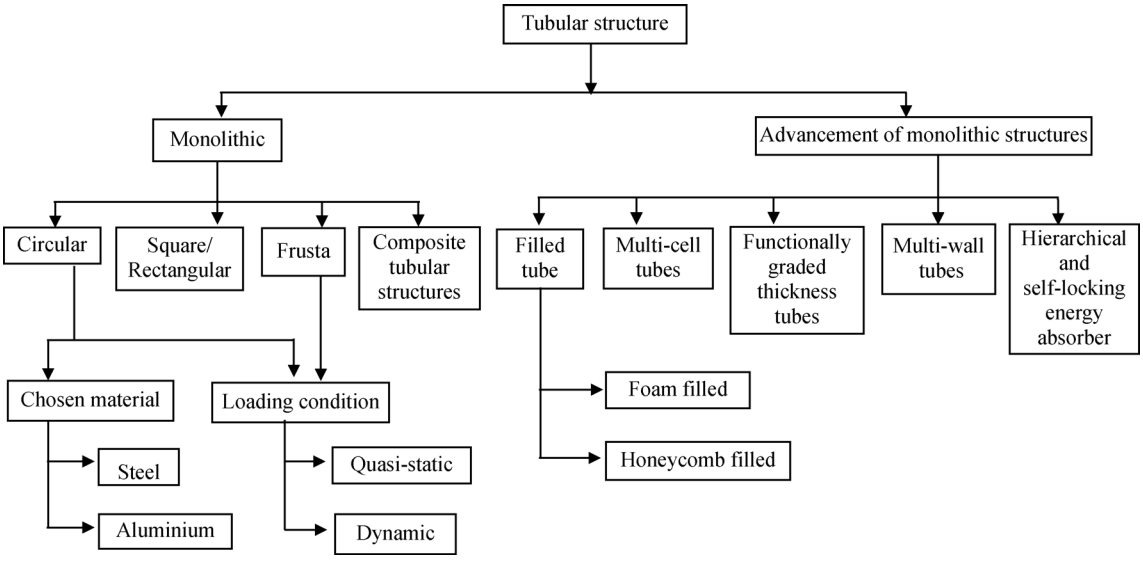

Fig. 2 Classification of a tubular structure.

• Density should be increased to avoid the time step problem.

Clausen et al. [4] overcame the problem of simulation time by introducing mass scaling into LS-DYNA. Tarigopula et al. [5] introduced a velocity-ramping technique to analyze the behavior of structures under quasi-static loading in LS-DYNA. Velocity is ramped from initial velocity to appropriate velocity and remains constant throughout the analysis. A curve is defined by a half sine wave function to provide the velocity-ramping condition.

2.3 Prediction of energy absorption

A crushable component has a specific deformation characteristic, based on which the energy-absorbing capacity can be predicted. Deformation or failure can vary for different tubular structures made of various materials. Three methods (analytical, experimental, and simulation) are used by researchers to analyze the energy absorption capacity of tubular components. In the analytical approach, deformation modes are an important factor that predicts energy absorption capability. Abramowicz and Jones [6] considered two folding elements (Type-I and Type-II) for a corner tube, as shown in Fig. 3 [6], to predict energy absorption capacity.

The energy absorption for Type-I, i.e., in-extensional mode (E_1), is given by

$$E_1 = P_o\left(\frac{16NI_1r_t}{t} + 2\pi w + \frac{4I_3N^2}{r_t}\right). \tag{5}$$

For Type-II, i.e., extensional mode (E_2), it is defined as

$$E_2 = P_o\left(\frac{2\pi N^2}{t} + 2\pi w + \pi N\right), \tag{6}$$

where t signifies the thickness of the tube, $P_o = Yt^2/4$, r_t designates the radius of toroidal shell, Y denotes the yield strength of material, and I_1 and I_3 are a constant integral value that depends on cross-section.

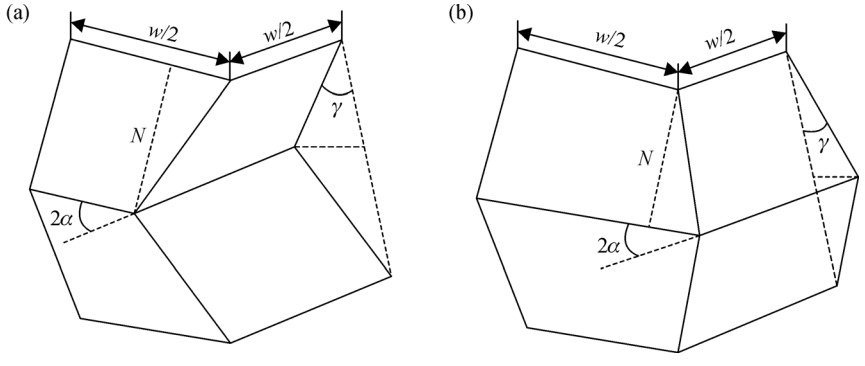

Fig. 3 Mode of collapse element: (a) Type-I and (b) Type-II. w: Width of the tube; α, γ: Folding angle of corner element; N: Distance between the plastic hinges of folding element. Reproduced with permission from Ref. [6] from Elsevier.

Energy absorption in the case of a Type-II folding element was rederived (Eq. (7)) by Abramowicz and Jones [7]. This improved kinematic mechanism consists of three forms of energy: Energy associated in extension, rebending of curved surfaces, and along the stationary hinge lines:

$$E_2 = 2P_o\left[\frac{4N^2\alpha}{t} + \pi w + N(\pi - 2\alpha)\right]. \quad (7)$$

Alexander [8] developed a theoretical model for a circular tube that deforms in axisymmetric or concentric deformation mode by considering inward folding. Thereafter, Abramowicz and Jones [9] derived an expression for the same deformation mode with inward and outward folding to determine energy absorption capacity. The authors considered two forms of energy: one is associated with plastic hinges (E_3) during the formation of one lobe (Eq. (8)) and the other one is associated with circumferential forces (E_4) (Eq. (9)):

$$E_3 = 4\pi P_o\left(\pi\overline{R} + N\right), \quad (8)$$

$$E_4 = 2\pi YtN^2\left(1 + \frac{N}{3\overline{R}}\right), \quad (9)$$

where $\overline{R}$ represents the mean radius of circular column.

Hong et al. [10] experimentally and numerically discussed the collapse modes for triangular tubes. The authors incorporated a multi-corner folding mechanism proposed by Wierzbicki and Abramowicz [11,12] to derive the mathematical expression for triangular tubes. The four collapse modes for triangular tubes were suggested, and then the authors derived the analytical expression for mean load based on the folding mechanism of each mode. The triangular tubes frequently exhibited Mode *C* collapse; for thick walls, Mode *B* collapse was observed. The expressions derived for Modes *A* and *B* provided lower and upper limits for the mean force, respectively.

For Mode *A* (all three edges move outwardly),

$$\frac{\overline{F}}{P_o} = 26.66\left(\frac{w}{t}\right)^{1/3}. \quad (10)$$

For Mode *B* (all three edges move inwardly),

$$\frac{\overline{F}}{P_o} = 24.48\left(\frac{w}{t}\right)^{1/2} + 6.12. \quad (11)$$

For Mode *C* (one edge moves outwardly and the two others move inwardly),

$$\frac{\overline{F}}{P_o} = 34.04\left(\frac{w}{t}\right)^{1/3} + 2.84\left(\frac{w}{t}\right)^{2/3} + 2.1. \quad (12)$$

For Mode *D* (one edge moves inwardly and the two others move outwardly),

$$\frac{\overline{F}}{P_o} = 35.16\left(\frac{w}{t}\right)^{1/3} + 3.85\left(\frac{w}{t}\right)^{2/3} + 4.17. \quad (13)$$

Apart from the two conventional folding mechanisms, i.e., extensional and in-extensional folding elements of tubes, a third inward-contracted folding element has been observed for triangular tubular structures [13]. Sun and Fan [13] explored the crushing behavior of triangular tubes under quasi-static loading via experimental and theoretical observations. The total five forms of energy (E_5) are associated with this third folding element and defined as

$$E_5 = P_o\left[3\pi N + 3\pi w + \left(\frac{2\pi}{3} + \sqrt{3}\right)\frac{N^2}{t}\right]. \quad (14)$$

Jones [14] introduced a concept known as the energy absorption effectiveness factor to evaluate a good component for absorbing impact energy. It is defined as the ratio of the total energy absorbed by the component to the energy absorbed up to the failure point by the same volume of material. A high factor is considered a good choice.

In experimental and numerical approaches, energy absorption can be predicted on the basis of the obtained load–displacement plot of tubular structures under compressive loading. Luo et al. [15] explored the response surface methodology to introduce a quadratic term that provides better result than the single-factor variation to obtain more accurate outcomes from a numerical approach [16].

3 Monolithic structures

Tubular structures are used as energy absorbers or as condenser–evaporator systems [17] in automotive applications. The major concern is how tubular structures absorb impact energy. Uniform and taper tubes with different cross sections, mostly circular, square, and rectangular, have been used to explore their energy absorption capability through experimental, numerical, and analytical approaches. This section summarizes the response of conventional tubular structures with reference to materials and loading conditions (quasi-static and dynamic).

3.1 Circular tube

Circular uniform cross-sectional tubes are widely used as absorbers because of their easy fabrication compared with other cross sections. The major parameters that determine the behavior of circular tube structures are diameter, height, thickness, and material. The deformation mode is a key indicator of the crashworthiness performance of structures. Available studies have reported three deformation modes by which kinetic energy dissipates during crushing. These deformation modes are

1) Concertina or axis-symmetric mode,
2) Diamond mode of collapse, and
3) Inversion and splitting of tubes.

3.1.1 Steel

Circular tubes made of mild, stainless (AISI 304), A36, and folding sheet steel have been examined against static and dynamic loadings.

3.1.1.1 Static loading

Studies on deformation patterns can be described properly under static loading compression. In 1960, Alexander [8] analyzed the crushing behavior of circular tubes, assumed the material as plastic rigid with plain strain condition, and provided an approximate analytical formulation (Eq. (15)) for mean load, which exhibited a good relationship with the results obtained from experimental tests.

$$\overline{F} = KYt^{1.5}\sqrt{\overline{D}}, \tag{15}$$

where K is a constant and $\overline{D}$ represent the mean diameter of tube.

The method used here was inapplicable to large deformations because it considered only a concertina mode.

Thereafter, Pugsley [18] provided an analytical relationship for mean load (Eq. (16)) that is applicable to a large deflection that reflects diamond modes:

$$\frac{\overline{F}}{F_{\mathrm{o}}} = 1.6 \times \frac{t}{R} + 0.12, \tag{16}$$

where F_{o} indicate the end load that causes yielding.

Alexander [8] considered stationary plastic hinges for the entire compression process. This work was modified by Wierzbicki et al. [19] to study moving plastic hinges through experimental observation. An earlier analysis was performed by considering assumptions of constant crush length for each crushing zone, which was not observed during the actual condition because of moving plastic hinges. Wierzbicki et al. [19] included a new term eccentricity described by parameter m, which showed the folding position with respect to the original radius of a tube. The eccentricity factor m was set as 0.5 for the folding that shared the same distance as the original position and as 0 and 1 for completely external and internal folding's, respectively. The crushing force for the entire crushing process was calculated using this arbitrary eccentricity parameter. Thereafter, Singace et al. [20] derived an eccentricity parameter and compared its value with the experimental findings.

Several modification techniques, such as providing cutouts, rings in the circumference of structures, and heat treatment, have been adopted by many researchers to provide a stable deformation mode. Gupta and Gupta [21] demonstrated the effects of annealing and cutouts on structures and found that the use of cutouts (Fig. 4) can prevent global buckling dominant in long tubes.

Gupta [22] studied the effect of cutout size by varying hole diameter and provided information regarding the deformation mode for tubes under annealed and non-annealed conditions. The non-annealed tube collapsed in concertina mode, and the annealed tube failed in diamond mode. Two opposite holes at mid height provided progressive deformation even for the case of a long tube, with the possibility of Euler buckling deformation mode. The presence of grooves throughout the surface at certain intervals also enhanced the performance of the structure [23]. The grooved tubes were analyzed through analytical [23] and experimental [24] approaches by varying the distance of grooves on the internal and external surfaces of the tubes. This process helped to control plastic deformation at a predefined interval, as depicted in Fig. 5(a) [24]. The implementation of short-interval grooves-controlled deformation, whereas long-interval grooves exerted no influence on the deformation pattern.

Mokhtarnezhad et al. [25] conducted experimental, numerical, and analytical investigations to explore the effect of an external grooved surface, as shown in Fig. 5(b). The grooved surface helped to provide an axisymmetric collapse mode that offered high load uniformity throughout the stroke length.

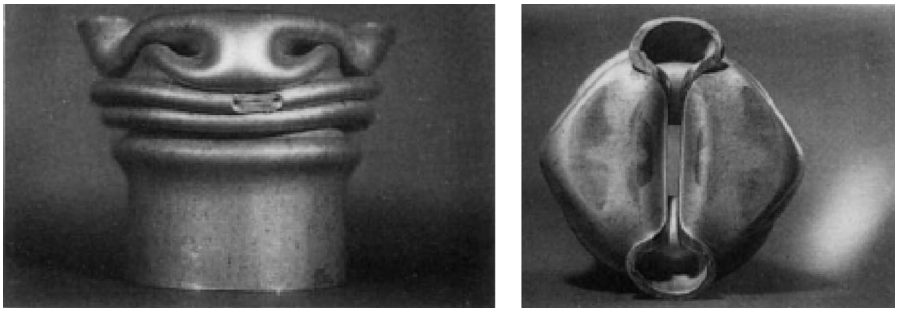

Fig. 4 Front and top views of a deformed tube with two opposite holes at mid height. Reprinted with permission from Ref. [21] from Elsevier.

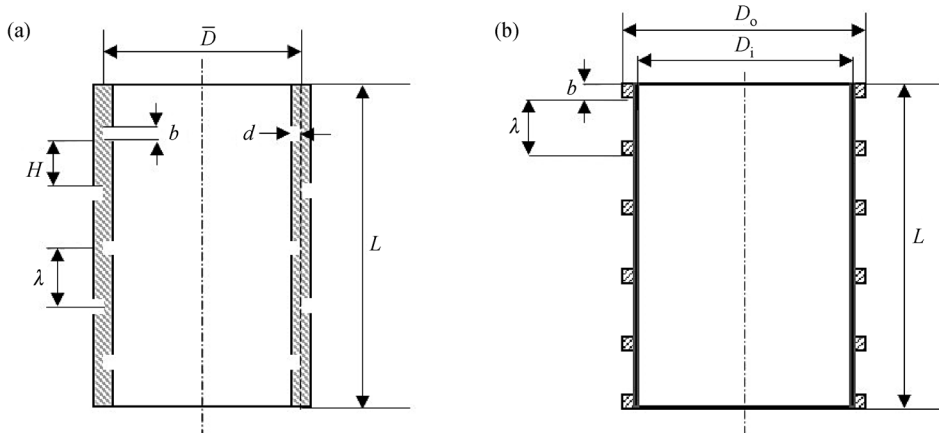

Fig. 5 Specimens with (a) alternative grooves [24] and (b) external grooves only [25]. $\overline{D}$, D_o, D_i: Mean, outer, and inner diameter of shell/tube, respectively; b, d: Width and depth of groove, respectively; λ: Groove distance; H: Length of rings between grooves. Reproduced with permission from Refs. [24,25] from Elsevier.

3.1.1.2 Dynamic loading

In case of quasi-static loading, approximate results are used to assess the initial stage of deformation characteristics of tubular structures. Dynamic loading, which reflects the actual condition by incorporating the inertia effect, is preferred to attain reliable results. The strain rate effect is a prominent factor under the dynamic loading condition. Karagiozova and Jones [26] studied the effect of strain rate on the crushing response of tubes under varying geometric and boundary conditions of the tubes along with impactor velocity. The obtained mean crushing load was predicted well using Alexander's modified theoretical solution [8], which included the strain rate sensitivity factor.

Wang and Lu [27] studied the crushing response of cylinder tubes (steel and aluminum) with a velocity range of 114–385 m/s and discovered a new deformation pattern known as the "mushrooming effect." With this effect, the wall of a tube thickened under dynamic loading, and various deformation modes were obtained at different velocity ranges, as illustrated in Fig. 6 [27].

Tabiei and Nilakantan [28] explored the effect of mine blasts underneath infantry vehicles on occupants. They adopted a new concept of energy-absorbing seat mechanism (EASM) that helps reduce reaction force by absorbing the kinetic energy of a blast from a mine underneath a vehicle. An analytical relation was developed and implemented to reduce the dependency on extensive computational studies and destructive testing. The trigger mechanism was also adopted by the authors of Refs. [29,30] to explore crushing behavior under dynamic loading. The effect of an elliptical cutout [29] on the surface of high-strength steel (HSS) tubes was studied using the finite element code LS-DYNA; cutout position and symmetry and variation in major axis were identified as the influencing parameters for the collapse behavior of structures.

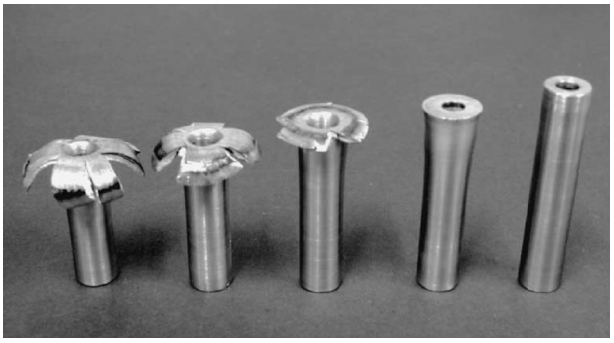

Fig. 6 Steel samples: Collapse modes at velocities of 385, 277, 227, 173, and 0 m/s (from left to right). Reprinted with permission from Ref. [27] from Elsevier.

A press-fitted steel ring around the circumference of a cylindrical steel tube was examined by Isaac and Oluwole [30]. These authors considered the effects of the parameters of ring thickness and number, slenderness ratio, and tube thickness, on the performance of the used structure under axial and oblique loading conditions, as shown in Fig. 7 [30]. The explicit finite element code ABAQUS using the Johnson–Cook material model was adopted for analysis. The tube with a ring exhibited better energy performance than the normal circular tubes.

3.1.2 Aluminum

Different forms of aluminum alloys (e.g., commercially available pure aluminum, AA-1050, AA-5052, AA-6060, and AA-6061, considering temper condition) were focused on in the present study for the crashworthiness performance of different tubular structures.

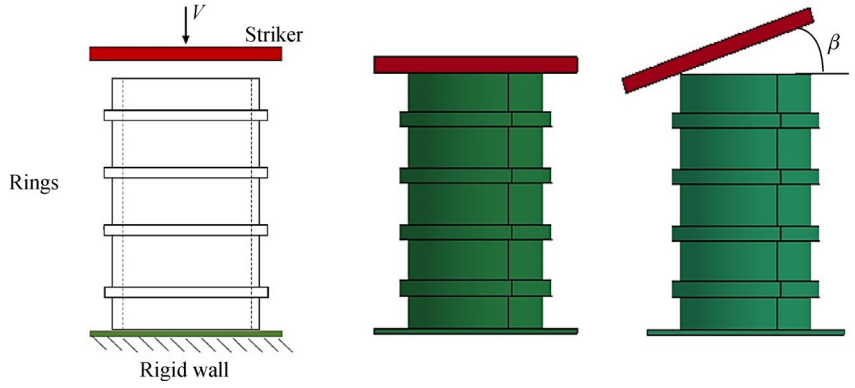

Fig. 7 Geometric configuration of the ring-fitted tube under axial and oblique loading conditions. V: Velocity of striker; β: Load angle. Reproduced with permission from Ref. [30] from Elsevier.

3.1.2.1 Static loading

The performance of tubes was analyzed with reference to cutouts, grooves, and heat treatment while designing the parts [24–26,31]. In several cases, the aluminum thin-walled structure exhibited opposing results to those of steel tubes. The specimens regarded as annealed deformed in concertina mode, and the non-annealed specimens presented a diamond deformation mode. The effect of cutouts on components made of aluminum displayed the same behavior as that of steel tubes.

Chen and Ozaki [32] provided corrugation on the circumference of a cylindrical structure, which reduced fluctuations in the load–displacement curve. Eyvazian et al. [33] studied two types of corrugation, i.e., radial corrugation (Fig. 8(a)) and longitudinal corrugation (Fig. 8(b)), with variations in corrugation depth and size on circular aluminum tubes to demonstrate the failure mode of the structures.

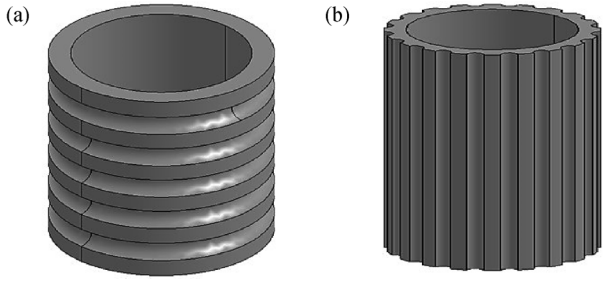

Fig. 8 Schematic of circular tubes with (a) radial corrugation and (b) longitudinal corrugation.

Experimentation demonstrated that the radial corrugation provides a low initial peak force because it acts as a buckling initiator with minimal load fluctuations. By contrast, the lateral corrugation presents a higher peak force value with more fluctuations in the load–displacement curve.

Other studies have been conducted to improve the energy absorption capacity of structures. Salehghaffari et al. [34] introduced two novel structural enhancement approaches to improve the crashworthiness of metal tubes. In the first design, shown in Fig. 9(a) [34], two tubes with interference theory were developed, in which a steel tube was used as the ring that was driven into the aluminum tube to expand the tube. Energy dissipated in three forms: Expansion of the aluminum tube, friction between the aluminum and steel rigid tubes, and the formation of a plastic concertina fold. The second layout, shown in Fig. 9(b) [34], was developed by generating grooves on the tube's surface to achieve progressive folding that will help enhance crashworthiness performance.

Nia and Khodabakhsh [35] explored the effect of radial distance on the crushing behavior of an aluminum AA-1050 circular tube that was tested experimentally and numerically. This radial distance, called dimensionless number (η), was calculated in terms of the outer radius (R_o) and inner radius (R_i) of the tube, as shown in Eq. (17):

$$\eta = \frac{2(R_o - R_i)}{R_o + R_i}. \tag{17}$$

The result indicated that if the value of η was between 1.2 and 1.52, then the structure exhibited maximum energy absorption; if η was 0.66, then the maximum specific energy was presented. Although the aluminum tube demonstrated good performance under the impact, the primary concern was the high initial peak force, which caused severe injury to occupants. Focusing on this issue, Ghamarian and Abadi [36] and Kumar et al. [37] studied the effects of a capped cylindrical tube under quasi-static axial loading on deformation mode and energy absorption capacity. The obtained results of the capped tube through experimental and numerical analyses were compared with those of an open-end tube. The initial peak was reduced by 15%–30% for the end capped tube compared with the

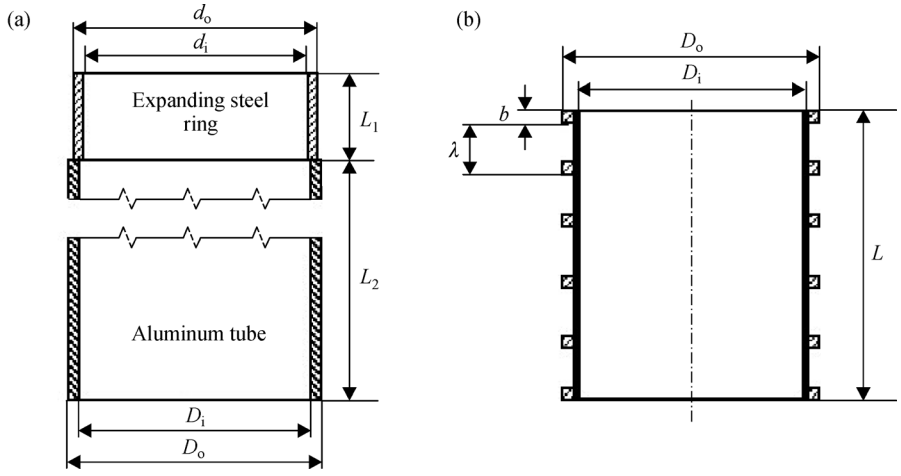

Fig. 9 Schematic of specimens with developed designs of (a) tube with expanding rigid ring press-fitted at the top and (b) tube with wide external grooves. d_o, d_i: Outer and inner diameter of expanding steel ring; L_1, L_2: Length of tubes. Reproduced from Ref. [34] from Elsevier.

conventional open tube, with identical energy absorption capacity.

Modifications in terms of triggering mechanism have been introduced to achieve the smooth plastic flow of tubes. Airoldi and Janszen [38] introduced a triggering mechanism into a hollow tube, which was part of the landing gear of an aircraft. This mechanism reduced the maximum initial peak force when impact occurred, which was useful for the crashworthy analysis of landing gears. The buckling initiator [39], as shown in Fig. 10 [39], was used as another means to reduce the initial peak during impact for landing gear applications and other roadside energy absorber applications.

Liu and Day [40] described the bending collapse behavior of a tube through global energy theory. The key parameters for deriving an empirical relationship were applied moment and bending angle, assuming that all crush energy was absorbed and distributed along the formed plastic hinge line.

Fig. 10 Circular tube with buckling initiator. Reprinted with permission from Ref. [39] from Elsevier.

3.1.2.2 Dynamic loading

Compared with steel, aluminum experiences less strain rate effect under dynamic loading condition [24]. The fatigue life of AA-7050-T7451 was examined through the continuum damage mechanism model [41] with the help of the obtained plastic flow through the impact of pit, residual stress, impact pit radius, and depth.

Galib and Limam [42] performed experimental and numerical analyses on an AA-6060-T5 circular tube with an impact velocity of 60 km/h. The major observation was focused on initial peak load, D/t ratio, and deformation pattern. The numerical results for the mean crushing force exhibited good correlation with the experimental results given that D/t ratio varied from 10 to 65. In case of dynamic loading, mean force increased by up to 10%. The effect of a buckling initiator [43] on two types of hat cross sections, i.e., bonded- and riveted-type tubular structures made of AA-1050 and AA-5052, was studied. The bonded structure provided better results because its increased crush strength compared with the riveted type. Wang and Lu [27] demonstrated the mushrooming effect on aluminum and found that it exhibited less strain rate sensitivity to all deformation features, similar to a steel tube. Figure 11 [27] shows the mushrooming of aluminum tubes at different velocities.

3.2 Square/rectangular tube

Energy absorbers have extensive application areas, and structure shape will change in accordance with the

Fig. 11 Aluminum samples: Collapse mode at velocities of 361, 220, 137, and 0 m/s (from left to right). Reprinted with permission from Ref. [27] from Elsevier.

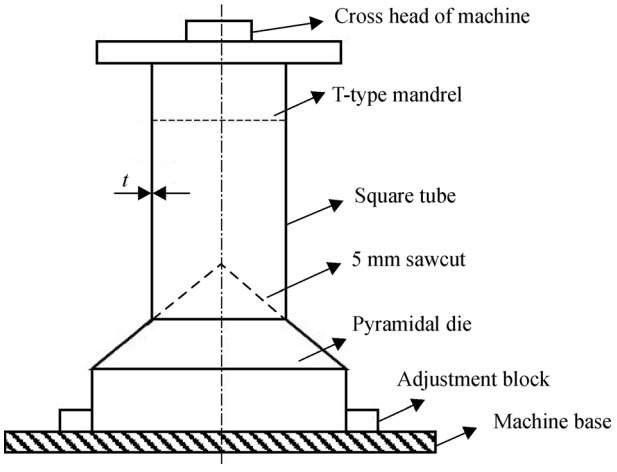

Fig. 12 Schematic representation of tube splitting arrangement. Reproduced with permission from Ref. [45] from Elsevier.

requirements of a particular application. Therefore, researchers have focused on structures other than the conventional circular tubular structure. This section includes detailed information regarding tubular structures with square/rectangular cross sections fabricated via the extrusion or welding of wall sheets. Studies are categorized on the basis of material and loading condition.

3.2.1 Steel

3.2.1.1 Static loading

Lu et al. [44] investigated the effect of splitting on the capability of structures to absorb impact energy apart from the earlier studied form of deformation to absorb energy. In their study, a structure with a square cross section absorbed energy in three forms: energy associated with the splitting of the tube at the starting point of contact that led to fracture initiation, progressive deformation with curl formation as friction energy, and tearing energy. Huang et al. [45] predicted the energy absorption of a tube splitting (i.e., tearing energy, friction energy, and bending energy) mechanism with theoretical formation and compared it with the experimental output. Three semi-angles (45°, 60°, and 75°) were selected for the pyramidal die on the tube splitting test, the arrangement of which is shown in Fig. 12 [45]. The results suggested two methods for increasing the *SEA* of square tubes: By increasing shell thickness and by providing curvature on a die instead of a sharp die.

During an actual crash, energy absorbers are subjected to axial loading, followed by bending collapse. Under this condition, a crash box system fails because of the axial force and bending moment. Han and Park [46] studied the effect of oblique loading on a mild steel thin-walled column that collapsed due to axial and bending effects. The theoretical expression for mean crash load was obtained in terms of geometric parameters and critical angles, which provided a good correlation with the experimental findings.

DiPaolo et al. [47] experimentally investigated the axial collapse behavior of a welded AISI 304 stainless steel square tube. The primary objective was to achieve a suitable configuration that could influence the structure's folding formation during crushing. Deformation control methods, which were in the form of grooved patterns on the sidewalls of the structure, as shown in Fig. 13(a) [47], and end constraint, as shown in Fig. 13(b) [47], provided stability to the load–deflection curve.

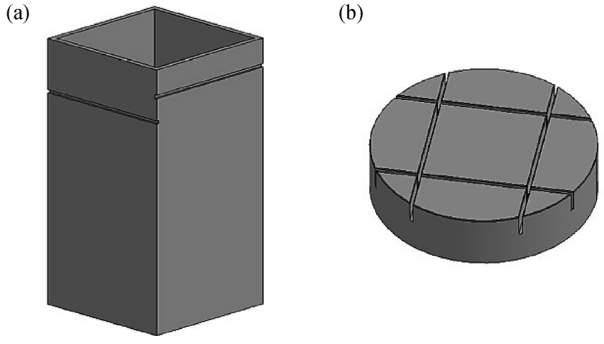

Fig. 13 Constraint used for a square box component: (a) Grooves on the sidewalls of the tube and (b) grooved end cap for end constraint. Reprinted with permission from Ref. [47] from Elsevier.

Xu et al. [48] investigated the crushing response of a tailor-welded blank (TWB) HSS tube structure that was fabricated via a laser welding process with different weld line locations. The TWB structure used in the study was not joined at the center but supported by two opposite plates. The effects of weld line location and material combination on the response of crashworthy parameters were studied. The result showed that the angle between the

weld line and the crushing position was a significant parameter.

3.2.1.2 Dynamic loading

Square tubes were analyzed experimentally, followed by a theoretical prediction [6,7] under dynamic loading. Strain rate affects the quasi-static compression of steel tubes. The obtained deformation of different samples showed that the unstable collapse behavior offered minimal plastic hinges that initiated buckling. Otubushin [49] used the experimental result mentioned by Abramowicz and Jones [6] to validate nonlinear finite element results, in which an isotropic elastic material model with strain hardening was selected and the Cowper–Symonds equation was used.

A hat-shaped square crash box system was investigated in Ref. [50] to predict the effect of combined elasto-plastic condition at the time of impact and strain rate sensitivity. The authors found that buckling occurred on opposite sides of the crash system under dynamic condition. This phenomenon can be avoided by using high plastic stress with a high-strain-rate material.

Gümrük and Karadeniz [51] introduced the geometric feature of a trigger bump (semicircular cross section) into a square hat crash box system (Fig. 14) and analyzed its crashworthy property by performing a simulation. Deformation behavior improved by using the trigger. Further simulation was performed to determine the effects of trigger position, size, and number on the crush response of the structure.

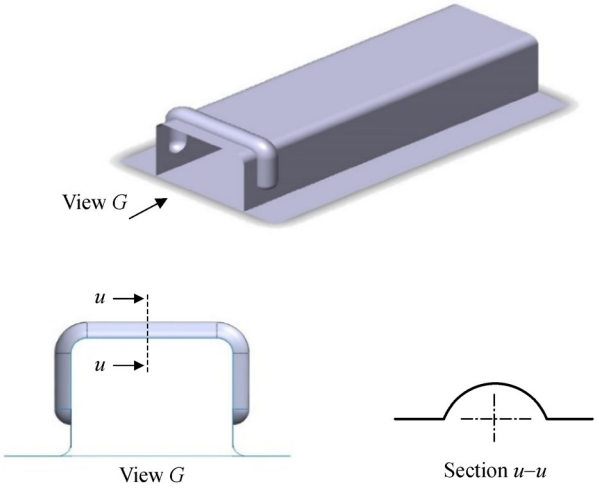

Fig. 14 Square hat tube with trigger. Reproduced with permission from Ref. [51] from Elsevier.

Zhang and Huh [52] investigated the performance of a square tube structure with longitudinal grooves on all its faces, as shown in Fig. 15(b) [52], and one with longitudinal grooves on opposite faces, as shown in Fig. 15(c) [52]. A series of simulation tests with an impact velocity of 10 m/s was performed, and the energy-absorbing characteristics were compared with those of a simple square tube, as shown in Fig. 15(a) [52]. Deformation behavior was defined in terms of E_{ab}, *SEA*, and F_{max} with variations in tube width, groove length, and groove number. Along with E_{ab}, *SEA* was enhanced by up to 82.7% and peak load was decreased by up to 22.3% compared with those of conventional tubes.

3.2.2 Aluminum

3.2.2.1 Static loading

Langesh and Hopperstad [53] studied the performance of extruded aluminum AA-6060 with variations in thickness and temper conditions (T4 and T6). The deformation modes were symmetric, which was primarily due to the temper condition of the alloy. The model of Abramowicz and Jones [6] was used to evaluate mean crushing load, which was considered satisfactory. Thereafter, numerical validation [54] was performed, and the result was compared with the result of [53] to compare the accuracy of the theoretical prediction and the assumption made in relation to extrusion geometry and temper condition. The results were compared with the experimental results, showing that the peak and mean load were approximately less than 10%. Jensen et al. [55] used AA-6060 with temper condition T6 to study different aspects of deformation, i.e., the transition of progressive deformation to global buckling with varied lengths. The local (b/h ranges from 17.78 to 40) and global (L/b ranges from 5 to 24) slenderness variables were important factors that marked critical global slenderness. They were described as deformation states with either a direct global buckling or a change from progressive to global buckling.

Tubular structures can absorb energy via piercing deformation mode. In this method, energy dissipation is achieved with the involvement of fracture or the tearing of structures at the contact point, leading to continuous stable curling. Stronge et al. [56] experimentally studied the effect of tube splitting on a square tube, in which energy dissipated in the form of fracture energy as the tube was pierced. This system predicted the energy associated with plastic deformation and the energy due to frictional work but hardly identified the tearing energy at four corners, which was the focus of Lu et al. [44]. Huang et al. [45] investigated the splitting of a square aluminum tube and provided the change in die shape (pyramidal die) used by Stronge et al. [56].

The effects of oblique and axial loadings are considered important parameters for analyzing the crushing response of energy absorber components. Reyes et al. [57] experimentally and numerically investigated oblique loading effect on an aluminum AA-6060 square tube

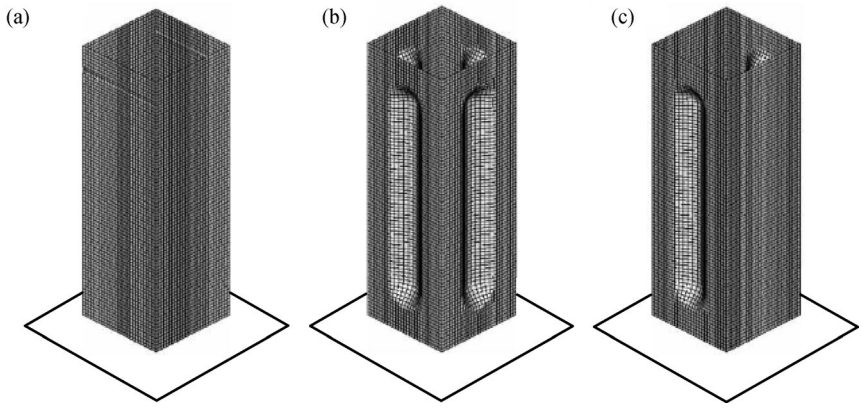

Fig. 15 Numerical models of (a) conventional square tube, (b) square tube with grooves on all faces, and (c) square tube with grooves on opposite faces. Reprinted with permission from Ref. [52] from Elsevier.

structure. The oblique impact condition was analyzed with three impact angles (5°, 15°, and 30°) measured from the center line of the structure. The result showed that energy absorption dropped drastically by introducing a 5° load angle; further increase in load angle led to compact energy absorption. Under oblique loading, a uniform structure collapsed in Eulerian buckling mode; consequently, it did not absorb impact energy up to the survival of occupants. Therefore, structures under such loading should be appropriately designed to reduce the chance of Euler mode deformation, followed by stable folding during crushing. Nia et al. [58] introduced a buckling initiator into a tube structure to avoid Euler mode and then tested it experimentally and numerically under oblique loading condition. The initiator was used in the form of cutting at the tube corner (Fig. 16) [58].

The effects of the position and number of initiators were the focus of their study. The authors found that the deformation mode changed from normal buckling to progressive buckling with the use of initiators. Zhang et al. [59] developed two types of patterns that were constructed using pyramidal elements, as shown in Fig. 17(a), on a square tube. Type A, as presented in Fig. 17(b) [59], was used to trigger the extensional mode, which was applicable to thin tubes. Type B, as shown in Fig. 17(c) [59], was for absorbing more energy with the formation of a new octagonal deformation mode. The obtained results showed that Type A absorbed 15%–32.5% of energy, and Type B exhibited an increased value of 54%–93% compared with a conventional tube.

Arnold and Altenhof [60] conducted a quasi-static experimental test on aluminum AA-6061 with temper conditions T4 and T6 and a hole discontinuity (Fig. 18) at the mid length of the tube. Under T4 condition, the tube was deformed in a progressive manner. Cracking with splitting led to a deformation under T6 condition. With the same geometric features and loading condition, AA-6061-T4 absorbed approximately 80% more energy than AA-6061-T6.

Cheng et al. [61] focused on the crush behavior of AA-6061-T6 with three geometric discontinuities: circular, slotted, and elliptical holes. *CFE* and *SEA* were improved

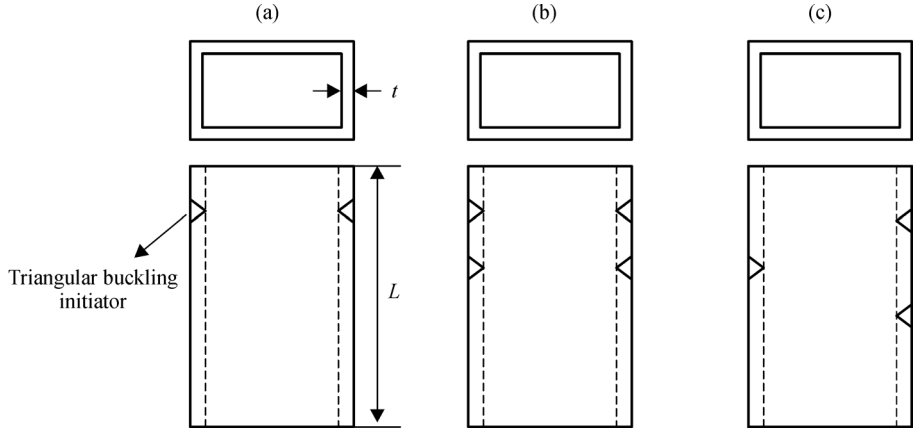

Fig. 16 Schematic of square tubes with different trigger positions: (a) Trigger at the top, (b) trigger symmetric on two planes, and (c) trigger asymmetric on three planes. Reproduced with permission from Ref. [58] from Elsevier.

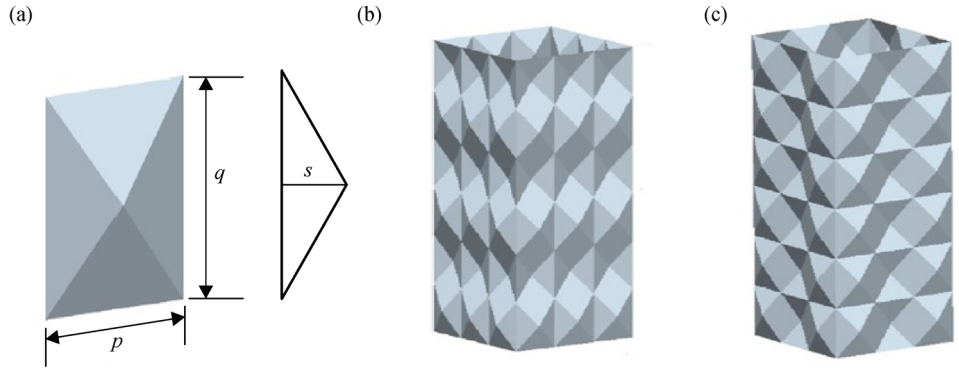

Fig. 17 Schematic of new design structure: (a) With pyramidal element, (b) Type A, and (c) Type B patterns. p, q: Side of pyramidal element; s: Apex height. Reproduced with permission from Ref. [59] from Elsevier.

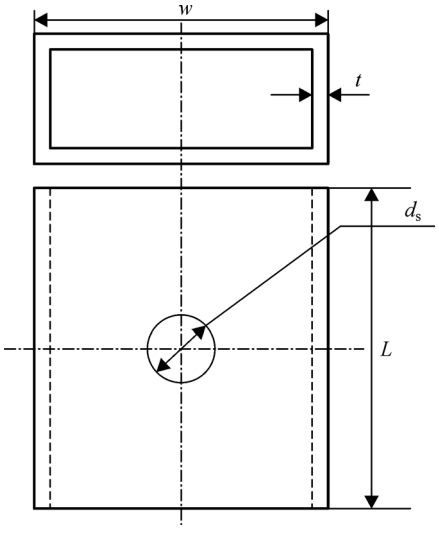

Fig. 18 Schematic of a square tube with a hole at mid length. d_s: Slot diameter. Reproduced with permission from Ref. [60] from Taylor & Francis.

with the use of cutouts but peak force was reduced compared with those of a conventional tube. Zhang and Zhang [62] performed experimental and numerical tests on AA-6061-O square tubes with varying thicknesses. The crushing performance of the square tube was explored through the identified collapse mode and the crush resistance provided by corner elements.

3.2.2.2 Dynamic loading

For identical crushing lengths, aluminum tubes exhibit higher mean force against impact loading [53] compared with that against static loading. Meanwhile, impact velocity does not significantly affect the variation in force [6]. A linear relationship was observed between energy and displacement under T4 condition, but the same energy level was determined for the T6 scatter pattern. The experimental results were predicted well by performing a simulation in Ref. [54]; a parametric study that explores crashworthiness performance by optimizing constrained parameters was emphasized. Fyllingen et al. [63] conducted stochastic simulation on a tube with a thickness of 3.5 mm subjected to dynamic loading. The results were compared with the experimental output [55]. They found a similar collapse mode (progressive buckling, global buckling, and transition phase from progressive to global) and maximum force, but the average force for the structure was underpredicted.

3.3 Frusta tube

The primary indicator for a good energy absorber is the load–displacement curve, which depends on all factors of crashworthiness being determined. Frusta tube structures exhibit a stable deformation curve, such as a uniform cross section, and demonstrate high response in case of large tubes due to their varying cross sections. Euler buckling occurs for uniform sections. The crushing response of frusta tubes under static and dynamic loadings is highlighted in this section.

3.3.1 Static loading

Mamalis and Johnson [64] investigated the response of an AA-6061-T6 annealed frusta or truncated-cone-type structure to explore the effects of taper angle (5° and 10°) and thickness. The experimental results were compared with those of a circular tube with the same height and outer diameter (larger end diameter for the frusta). The thick tube presented a concentric ring of folds, and the thin tube formed a diamond lobe after achieving initial first folding as an asymmetric mode of deformation. In addition to collapse mode, slenderness ratio ($t/\overline{d}$) also affected structure performance. Thereafter, Mamalis et al. [65] developed a theoretical model for peak force and mean force with the assumption that no change will occur in the

initial smaller diameter as it deforms. The obtained results and theoretical model were primarily affected by slenderness ratio and taper angle. With an increase in slenderness ratio (keeping mean diameter constant while thickness increased), peak force also increased. A small increment in mean force caused a large variation in load amplitude in the load–deformation curve. As the taper angle increased (5°, 10°, and 14.35°), the peak force decreased. The mean force was minimally affected, followed by a progressive collapse that reflected an increase in *CFE*. Reid and Reddy [66] explored the effect of a mild steel square tube with tapered faces on the response behavior of the load–deformation curve under quasi-static and dynamic loading conditions. Two distinct models, i.e., single-tapered and double-side tapered tubes, were compared with a uniform straight tube. The tapered tubes exhibited better stability in the load–deformation curve.

In a similar context, Nagel and Thambiratnam [67] performed a parametric study by using the finite element code ABAQUS to demonstrate the performance of a rectangular frusta tube with double taper, triple taper, and all-four-side taper. Along with the variation in faces, varying thicknesses and semi-apical angles were also considered for the analysis under quasi-static axial loading. The initial peak load increased significantly with an increase in wall thickness and decreased with an increase in taper angle. References [36,37] focused on the deformation characteristics of a circular end capped tube and found that the capped structure reduced the initial maximum load by 15%–30% compared with an uncapped tube. The researchers adopted capped and uncapped structures on frusta tube to explore its crashworthy properties under quasi-static and dynamic loading conditions.

El-Sobky et al. [68] highlighted the influence of a capped end or a constrained structure by performing a quasi-static experimental test. Four types of constrained motion were studied: (1) Top constrained, (2) base constrained, (3) fully constrained, and (4) non-constrained frusta. Among all the constrained structures, the top-constrained frusta achieved maximum energy absorption by providing a radial end constraint. The influences of semi-apical angle (15°–60°) and thickness (1–3 mm) on the crushing response of frusta tubes were studied by Alghamdi et al. [69]. Five types (Mode-I, Mode-II, Mode-III, Mode-IV, and Mode-V) of collapse modes were identified (Fig. 19) [69]. These modes were the combination of the lower end having an outward inversion and the upper end having an inward inversion and an extensible collapse.

Frusta with a tapered angle of 75° exhibit a folding crumpling deformation mode [70]. In this mode, the structure can absorb the maximum amount of energy compared with other deformation modes because plastic deformation is highly associated with the formation of a number of plastic hinges.

Gupta et al. [71] studied the influence of taper angle (16.5°–65°) on the deformation mode of an aluminum conical frusta tube. The experimental findings indicated that a diamond failure mode appeared for a taper angle of up to 30°. Meanwhile, frusta with higher taper angles (44.8°, 53°, and 65°) failed due to the formation of rolling and stationary plastic hinges. Increased taper angle resulted in increased proneness to the formation of plastic hinges, which led to maximum energy absorption. A cap surface also reduced the initial maximum force. In this context, modifications in geometry with variations in angle and structure were studied by Prasad and Gupta [72]. The authors conducted a comparative study of collapse modes and load deformation behavior of aluminum spherical domes and tube under quasi-static and dynamic impact conditions. The frusta geometry was varied as the taper angle increased from 44.5° to 67.1° and the slenderness ratio ($t/\overline{d}$) ranged from 0.00554 to 0.02152. For a hemispherical cap, R/t value ranged from 15.3 to 240.9. The deformation mode was sensitive to the compression rate. In case of a spherical dome and an increase in R/t value, mean collapse load increased; in case of frusta, mean load and energy absorption capability increased with an increment in d/t. Niknejad and Tavassolimanesh [73] introduced a mathematical model for the plastic deformation of a capped-end frusta tube with inversion collapse. The proposed analytical model was used to predict the instantaneous load versus displacement at the time of the inversion process.

The effect of geometric modification in the form of corrugation and cutouts has been studied for tapered tubes, as mentioned in the earlier section (circular and square/rectangular tubes), to explore their deformation behavior. Chahardoli and Nia [74] performed experimental and numerical analyses on the crushing response of a capped end taper tube made of steel alloy 430 with a circular hole. The variations in hole position, thickness, and diameter and the number of planes and holes in a plane were the most affected parameters for the collapse mode of the structure. The obtained results showed that an open-ended absorber exhibited better performance than cap-ended frusta. *CFE* and initial maximum force were affected by the variation in hole position. When a hole was located near the loading end, the initial peak force for open-ended and cap-ended frusta tubes decreased with an increase in *CFE*.

3.3.2 Dynamic loading

Mamalis et al. [75] investigated the response of a tapered tube under axial and oblique dynamic loading conditions. The collapse modes of a tapered tube with two semi-apical angles (5° and 10°) were compared with the those of a uniform circular tube. The effects of $t/\overline{d}$ and taper angle were highlighted while explaining the deformation pattern. The peak load increased with an increase in $t/\overline{d}$ but

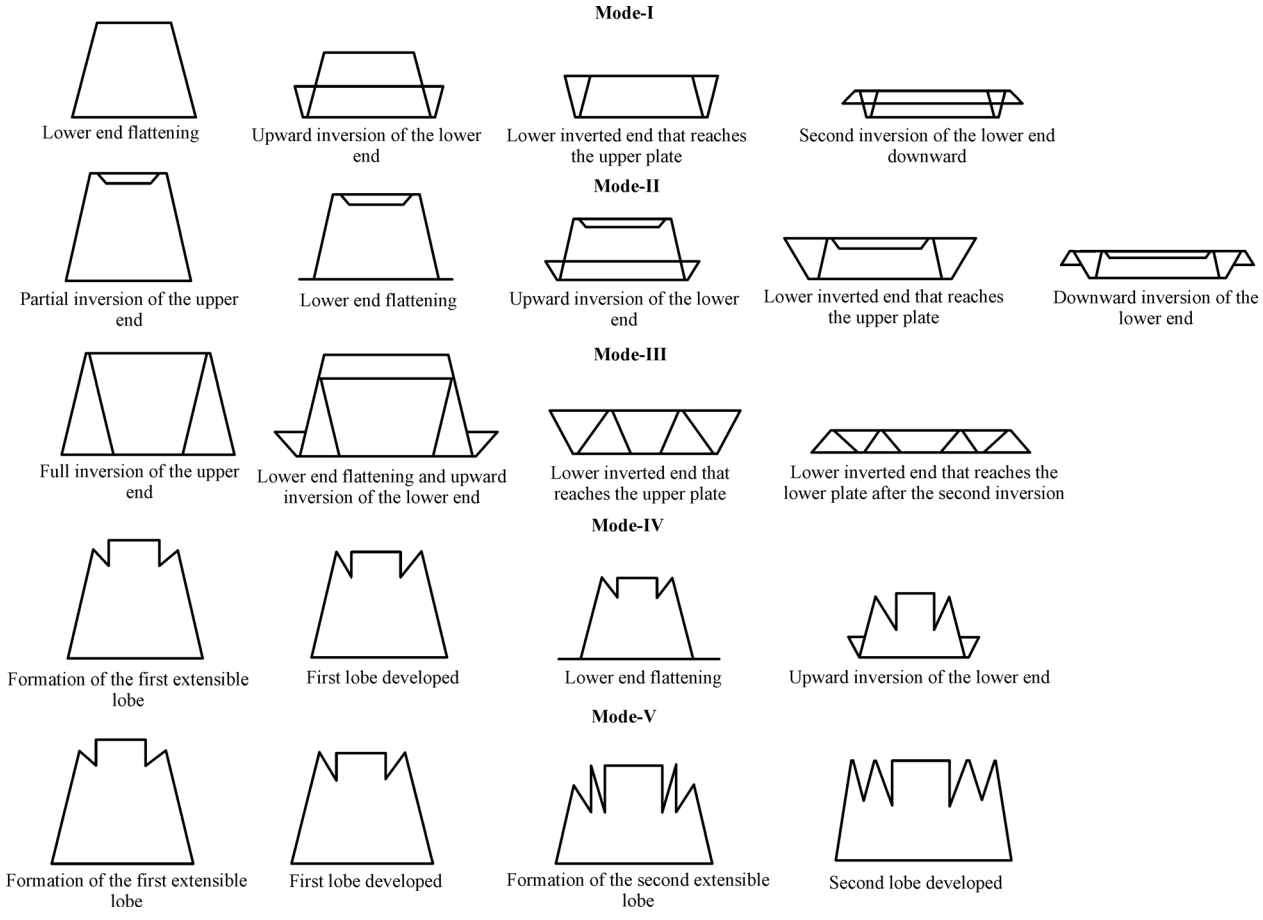

Fig. 19 Mechanism of deformation. Reproduced with permission from Ref. [69] from Elsevier.

decreased with an increase in taper angle. Nagel and Thambiratnam [76,77] extended this work with variations in loading condition (impactor mass and velocity) and geometric features (thickness, tapered angle, height, and width of tube). The results were compared with those of a uniform rectangular section, and the researchers concluded that the tapered tube was more sensitive to thickness and impact velocity. Nagel and Thambiratnam [78] determined the crashworthiness performance of a tapered rectangular tube under oblique dynamic loading condition with variations in loading parameters (angle of obliquity and impact velocity) and geometric parameters (wall thickness, taper angles, number of taper faces, height, and width). An increase in load angle reduced the energy absorption capacity, which could be avoided with an increase in the number of taper faces. In addition to loading angle, thickness also influenced energy absorption during progressive collapse, but width and length were insignificantly dominant. The effect of geometric irregularities was also studied under dynamic loading condition. Taştan et al. [79] examined tapered tubes by introducing lateral circular cutouts as shown in Fig. 20 [79].

Simulations were performed using the finite element code LS-DYNA to explore the effect of lateral cutouts on crashworthiness performance. The authors focused on the surrogate-based optimization method to find the optimal value of properties and features, such as taper angle, cutout diameter, cutout position, and number of cutouts to obtain high *CFE* and *SEA*. *CFE* and *SEA* for taper tubes with cutouts increased by 27.4% and 26.4% compared with taper tubes without cutouts.

3.4 Composite tubular structures

The deformation behavior of structures made of composite materials differs from that of metallic ones. Composites are brittle and follow different energy-dissipating modes, such as through fiber breakage, delamination, and matrix cracks [80]. Metallic thin-walled components exhibit a ductile property and allow deformation through a controlled and progressive manner. Irrespective of the greater *SEA* of composite materials compared with steel and aluminum, they have a limited field of applications, such as the aerospace and sport car industries, due to their anisotropic behavior [81] and difficulty in design and analysis. The analysis of composite structures depends on fiber type and orientation, matrix resin type, and testing condition (temperature and load) that determine energy absorption

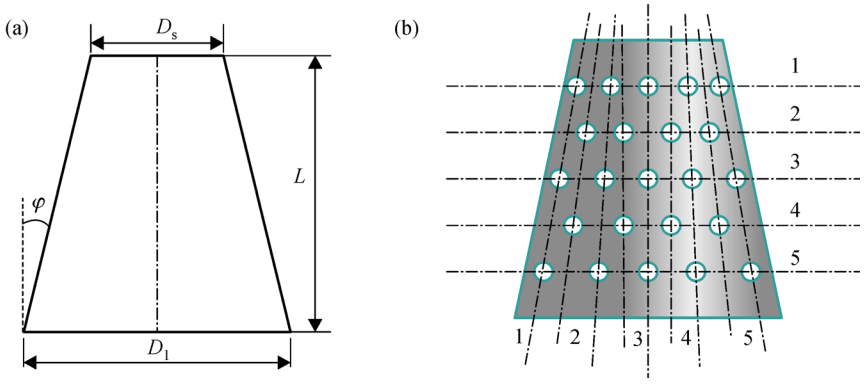

Fig. 20 Schematic of tapered tubes (a) without cutouts and (b) with circular cutouts. D_s, D_l: Smaller and larger end diameter of frusta tube respectively; φ: Taper angle of frusta tube. Reproduced with permission from Ref. [79] from Elsevier.

capacity and failure mode [82]. Solaimurugan and Velmurugan [83] studied the effects of fiber orientation and stacking sequence on the specific energy absorption capacity of a glass/polyester composite tube under axial compression.

Kim et al. [84] comparatively studied circular composite tubes with different reinforcing fibers (Kevlar, carbon, and carbon–Kevlar hybrid fibers) with epoxy resin. The experimental results showed that the carbon/epoxy tube exhibited better energy absorption capability than Kevlar. Hamada et al. [85] studied carbon fiber/polyether ether ketone tubes under a quasi-static axial compression test to acquire information regarding the formation of splaying mode. Song et al. [86] derived an expression for the instantaneous velocity and displacement of metal tubes (aluminum, copper, and steel as inner tube materials) wrapped by a glass/epoxy composite, which was validated with the experimental results. The quasi-static and dynamic compression tests demonstrated four similar modes of deformation, namely, compound diamond, compound fragmentation, delamination, and catastrophic failure, as shown in Fig. 21 [86].

Mirzaei et al. [87] developed an expression for a hybrid tube (aluminum tube wrapped with glass–epoxy composites) under quasi-static loading, which was based on Alexander's model [8]. The expressions for mean crushing force and fold length were derived by considering the effects of the stacking sequence of fiber, the ply orientation of each layer, composite and metal properties, the thickness of metal and composite, and other geometric dimensions. The composite structures are required to perform efficiently; two factors are important to achieve this objective: to initiate the failure of the structure by adopting trigger techniques and to maintain the stability of the crumble zone [88].

Thuis and Metz [89] discussed the splaying and fragmentation modes of the deformation of carbon/aramid hybrid composite components with trigger inclusion. The splaying mode absorbed more impact energy than the fragmentation mode. Siromani et al. [90] compared the effects of three trigger mechanisms (chamfered end, inward folding, and outward splaying crush caps) with the response of a flat-ended composite tube.

Huang and Wang [91] introduced a bevel trigger into a carbon-reinforced composite tube and analyzed its deformation behavior experimentally and numerically under quasi-static loading. The bevel trigger helped control the initiation of failure by reducing initial peak, enhancing its deformation stability. Chiu et al. [92] investigated the effect of tulip triggered on a carbon–epoxy composite tube subjected to quasi-static and dynamic loading having loadings with a strain rate of up to 100 s^{-1}. The authors concluded that the strain rate had no effect on the specific energy absorption capability of the composite because it

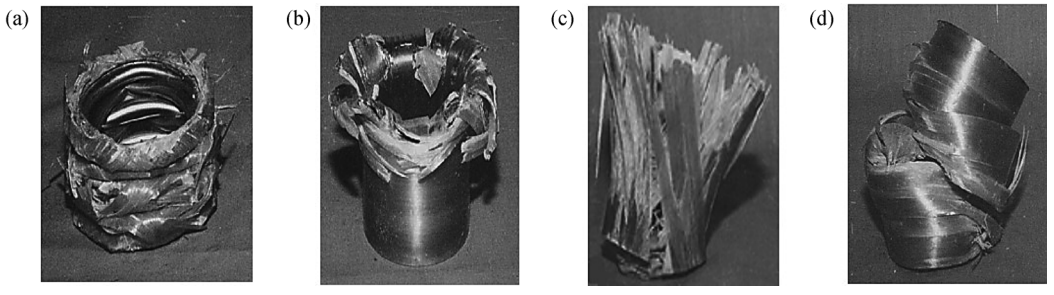

Fig. 21 Collapse modes of combined tube: (a) Compound diamond, (b) compound fragmentation, (c) delamination, and (d) catastrophic failure. Reprinted with permission from Ref. [86] from Elsevier.

completely depended on the manner of fiber failure propagation.

Similar to metallic tubes, composite tubes also provide corrugation for enhancing energy with the uniform deformation of structures. Mahdi et al. [93] numerically studied corrugation along a circumference of cotton fiber/propylene tube. Corrugation helped deform the structure at a predefined region, which continued to form progressive crushing. The energy absorption capability of such type of tube primarily depended on the number of corrugations provided on the shell and aspect ratio. The performance of a corrugated tube made of laminated woven roving glass fiber/epoxy was explored under axial [94] and lateral loading conditions [95]. The effect of corrugation in the radial direction was compared with that in a uniform composite tube under axial loading. The radial corrugated composite tube (RCCT) exhibited good energy absorption capability. In case of lateral loading, no significant effect on energy absorption was observed. The RCCT tube failed initially via debonding of the face surface, leading to the mushroom type of failure.

Apart from a circular cross section, square and rectangular sections fabricated with different composite materials have also been focused on in crashworthiness studies. Mamalis et al. [96] reported the crashworthiness behavior of square tubes fabricated with two composite materials: A fiberglass composite with random fiber orientation and a commercial glass fiber. The effects of variations in thickness and crushing length were studied under axial and dynamic loadings. Carbon fiber-reinforced plastic (CFRP) square tubes were analyzed under axial static compression [97] by considering the effects of the length, thickness, and volume of fiber and reinforcing plies, in addition to geometric aspect ratio and laminate properties. The brittle deformation formed was categorized in three modes (Fig. 22) [97]: Mode-I progressive end crushing, Mode-II local shell buckling, and Mode-III mid-length collapse. Among the three modes, Mode-I exhibited a stable deformation as failure due to the splaying and bending of laminates rather than shearing in the transverse direction.

Thereafter, the authors performed a dynamic test [98] to analyze the effect of strain rate. The studies conducted in the published literature [97,98] were validated by performing simulations [99] using the finite element code LS-DYNA 3D. Zarei et al. [100] numerically and experimentally explored the crushing behavior of a square tube made of a thermosetting composite by using the multi design optimization technique. The crashworthiness performance of the optimally designed composite tube was compared with that of an optimum aluminum tube. The energy absorption of the optimum composite tube was 17% more and it had 26% less weight than the optimum aluminum tube.

The nature of composite deformation is brittle; thus, considerable work has centered on how brittle structures can be turned into ductile structures. In this regard, Bambach et al. [101] worked on a composite steel–CFRP tube to achieve high energy absorption by combining the properties of steel. Bambach et al. [102] investigated a spot-welded square tube made of HSS reinforced with carbon fiber polymer (Fig. 23) under static and dynamic loading conditions.

The results were compared with the results of earlier studies mentioned in Ref. [103]. The steel with a spot-welded composite tube presented a fracture at the corner due to the wide range of spot weld that caused debonding and curling. Bambach [104] investigated different combinations of metal and composite. The author studied three combinations of metals, namely, steel, stainless steel, and aluminum, with a CFRP square hollow section (SHS) tube and compared the performance of different configurations. The result indicated that the strength, mean crushing force, and specific energy absorption improved by up to 1.9, 1.87, and 1.55 times, respectively, with the use of a CFRP–metal SHS tube. The bonding between the metal and the fibers was further investigated using an element approach (effective width method) [105].

4 Advancements in monolithic structures

Researchers have given considerable attention to thin-walled tubular structures, mostly circular and square

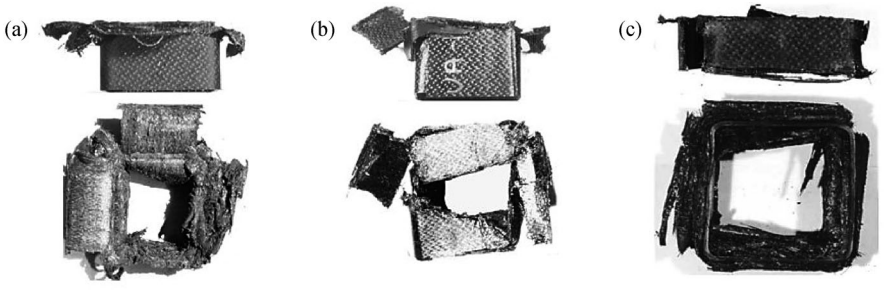

Fig. 22 Modes of failure of specimens under compressive loading: (a) Mode-I, (b) Mode-II, and (c) Mode-III. Reprinted with permission from Ref. [97] from Elsevier.

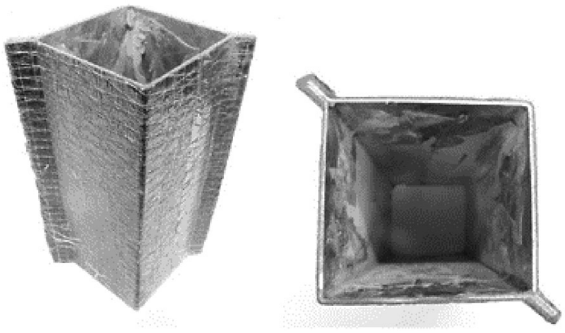

Fig. 23 Spot-welded steel–CFRP SHS tube. Reprinted with permission from Ref. [102] from Elsevier.

sections. With the advancement in numerical methods, researchers have progressed to exploring the deformation mechanism of complex structures.

This section focuses on modified structures that enhance crashworthiness performance under impact loading. Structures are modified with the addition of fillers (either foam or honeycomb) to conventional tubular structures (studied in Section 3), multicellular structures, multiwall structures, structures with functionally graded thickness (FGT), and hierarchical and self-locking structures.

4.1 Fillers used in tubular structures

Simple tubular structures have provided good results, as studied earlier, and should be further improved by filling additional structures. With the addition of fillers, individual performance improved the overall crashworthiness characteristics of structures. In this section, tubular structures filled with foam (either metallic or nonmetallic) and honeycomb core are studied.

4.1.1 Foam-filled tubular structures

The response of foam at different impact velocities should be identified for the efficient use as core in filled tubes' energy-absorbing components. In this context, Zheng et al. [106] explored the collapse characteristics of a metallic foam rod by using wave models. The behavior of stress, strain, and velocity in the foam rod during impact was derived by considering two wave models: Transitional mode for medium-velocity impact and shock mode for high-velocity impact. The authors considered two impact conditions: The impact of rod–target and the impact of striker–rod. Zheng et al. [107] further investigated a unified framework of plastic shock wave models to predict high-precision stress induced at the time of shock that arose from both impact conditions. The energy absorption capacity of cellular structures under dynamic loading is frequently integrated with three factors (inertia stability, shock wave effect, and material strain rate hardening), making the prediction of the dynamic effects difficult [108]. Liu et al. [108] developed a model that incorporated the three factors associated with micro lattice structures. They also explored the effects of individual factors through finite element method simulations.

Reid et al. [109,110] and Reddy and Wall [111] performed static and dynamic tests on polyurethane foam-filled square, rectangular, tapered, and circular tubes made of mild steel sheet. The load stability and energy absorption capacity were compared with those of an empty tube, and the effect of the interaction between the foam and metal was explained through theoretical models. The deformation in compact form rather than in non-compact form (Fig. 24) [109] as foam filler was used, which enhanced energy absorption two times, compared with an empty tube.

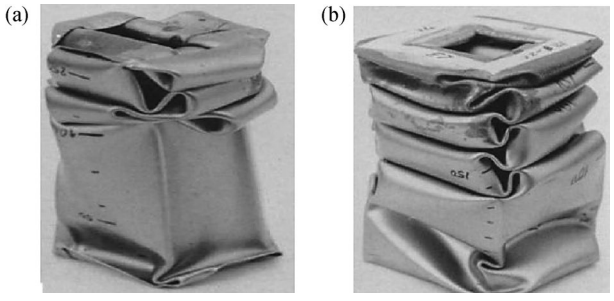

Fig. 24 Deformed specimens: (a) Non-compact form and (b) compact form. Reprinted with permission from Ref. [109] from Elsevier.

Seitzberger et al. [112] experimentally studied the crushing response of steel columns with three cross sections, i.e., square, hexagonal, and octagonal, filled with aluminum foam (Fig. 25). The analysis showed that the square section was a good choice compared with the hexagonal and octagonal sections.

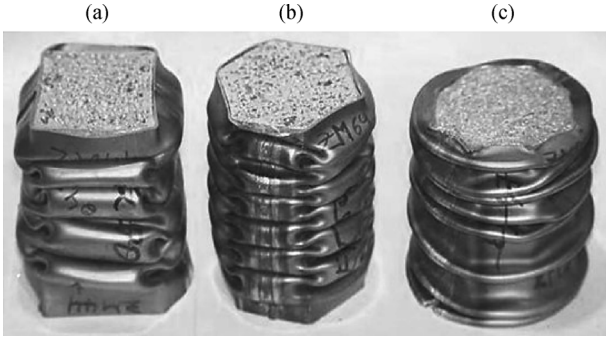

Fig. 25 Crushed specimens: (a) Square, (b) hexagonal, and (c) octagonal filled with aluminum foam. Reprinted with permission from Ref. [112] from Elsevier.

Güden and Kavi [113] explored the effect of a constrained structure (Fig. 26) filled with foam and without foam on deformation behavior. A quasi-static analysis was performed on a multi-aluminum tube filled

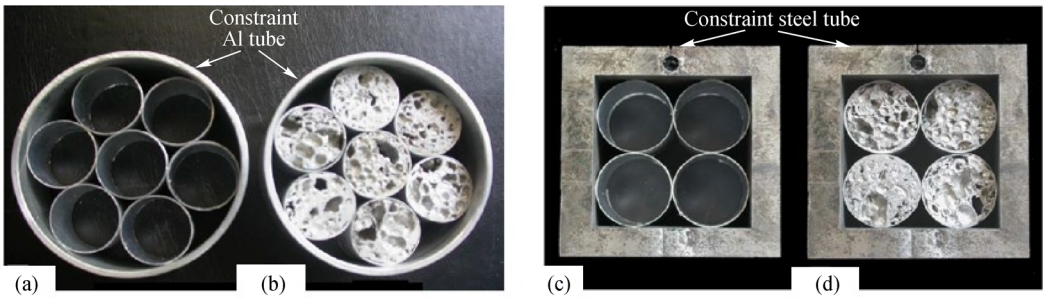

Fig. 26 Constrained multi-tube structure: (a) Hexagonal packed empty, (b) hexagonal packed aluminum foam filled, (c) square packed empty, and (d) square packed aluminum foam filled tube. Reproduced with permission from Ref. [113] from Elsevier.

with aluminum foam and empty tubes with square and hexagonal constraints. Comparative analysis showed that single tubes and multi-tubes with fillers provided better result than empty multi-tubes.

Abramowicz and Wierzbicki [114] studied foam interaction with a tube when compression occurred. The suggested approach was applicable to structures under static loading and could be incorporated for the stain rate effect by adjusting the flow stress of metal and foam. Seitzberger et al. [115] investigated the crushing response of a steel tube with aluminum filler. The interaction of the tube and the filler improved efficiency, which provided stability in deformation mode and enhanced the energy absorption capability of structures. The interaction of aluminum tubes filled with aluminum foam provided a thickening effect that helped convert diamond mode into concertina mode. Hanseen et al. [1] studied the conversion of this mode and found that foam density was the major deciding parameter. At critical density, modes were changed to concertina, which helped maintain load uniformity throughout compression. Similarly, concertina modes were observed in an aluminum tube filled with polyurethane foam at high densities of foam material [116]. Hanseen et al. [117] worked on the bonding effect of an aluminum foam-filled extruded square tube under a quasi-static experimental test. Apart from bonding influence, other important parameters, such as extruded wall thickness, cross section, wall material, and foam type and density, were investigated. Thereafter, Hanseen et al. [1,118] reported the effects of dynamic loading on square and circular foam-filled tubular structures with the addition of a trigger. The results indicated that the strain rate sensitivity of the foam-filled structures exhibited minimal dependency, similar to non-filled structures. A theoretical model was also developed to calculate mean crushing force. The theoretical model, i.e., Eq. (18), for the average crushing force of foam-filled structures (F_a^f) consists of three parts. The first part showed the mean crushing force for an empty tube ($\overline{F}$), the second part showed the plateau stress (σ_p) of the foam, and the third part showed the interaction effect. This equation exhibited agreement with the experimental results.

$$F_a^f = \overline{F} + \frac{\pi}{4}\sigma_p w^2 + C_a\sqrt{\sigma_p \sigma_o w}t, \tag{18}$$

where σ_o represents the extruded wall stress.

Equation (18) was derived by Santosa et al. [119] based on simulation results to find the mean force of a square tube structure. Structure performance was studied with two cases: By adhesive and by providing friction between the filler and the tube. A strengthening coefficient (C_a) was considered in Eq. (19), with a value of 1.8 for unbounded (providing friction) and 2.8 for bonded (providing adhesive).

$$F_a^f = \overline{F} + \sigma_p C_a b^2. \tag{19}$$

Kavi et al. [120] predicted the energy absorption capability and deformation mechanism of different foam (aluminum and polystyrene)-filled structures (Fig. 27)

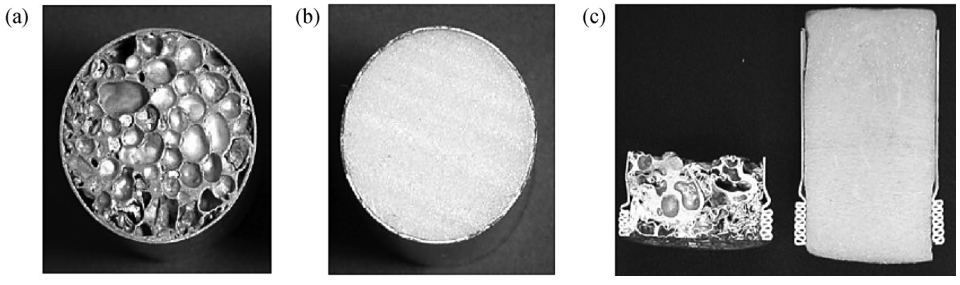

Fig. 27 (a) Aluminum foam-filled tube, (b) polystyrene foam-filled tube, and (c) concertina collapse mode. Reprinted with permission from Ref. [120] from Elsevier.

[120]. With the use of foam filler, the diamond deformation mode that was dominant in empty tubes changed to the concertina failure mode, as shown in Fig. 27(c) [120]. An analysis of the foam filler was also performed on a tapered tube given that it exhibited good characteristics of deformation behavior, as studied in the earlier section.

Mirfendereski et al. [121] numerically investigated the performance of rectangular tapered tubes (double, triple, and four tapers) made of mild steel filled with polypropylene foam under static and dynamic loading conditions. The effect of wall thickness was more important than that of taper angle on the deformation behavior of the foam-filled structures; for energy absorption capability, both parameters exerted the same importance. Ahmad et al. [122] studied the effect of foam-filled conical tubes, as shown in Fig. 28(a) [122], under oblique dynamic loading condition, as shown in Fig. 28(b) [122], and presented the energy response by considering the angle of obliquity and other geometric variations (wall thickness, taper angle, and tube height). Energy absorption for the foam-filled conical tubes was maximum at a taper angle of 5° compared with an empty tube.

The filler material should exhibit good capability to absorb impact energy, along with low density and light weight. Meguid et al. [123] conducted experimental and simulation studies on an ultralight foam-filled tubular structure, in which PVC foam as filler (tubular cross section with different internal radii) and an aluminum tube with a thickness variation of 0.1–0.5 were used. Relative stiffness was studied with reference to the internal radius of the foam and tube thickness.

4.1.2 Honeycomb filler

Santosa and Wierzbicki [124] conducted a comparative study of aluminum honeycomb- and aluminum foam-filled square tubes in terms of weight and solidity ratio (ratio of thickness to width) under quasi-static loading using the nonlinear finite element code PAM-CRASH. In the case of the honeycomb filler, the strength-to-weight ratio was higher when the solidity ratio was greater than 1.2%; for the foam filler, the solidity ratio increased by up to 2.3%. The aluminum honeycomb filler was more efficient in weight than the foam filler. However, under combined loading (compressive + bending), the structure with aluminum foam provided better result than the aluminum honeycomb filler because honeycomb only performed better under unidirectional loading.

Zhang et al. [125] compared the different honeycomb sandwich columns shown in Fig. 29 [125] (Kagome, triangle, hexagon, square-3, square-4, and diamond) with a foam-filled tube by considering the adhesive effect on the energy absorption capability of the structures. The tube with Kagome honeycomb sandwich core was found to be a better energy absorber, and the quadrilateral composite column exhibited less value.

Yin et al. [126] numerically analyzed the crashworthiness response of honeycomb-filled single and bi-tubular polygonal tubes, as shown in Fig. 30 [126]. The multi-objective particle swarm optimization technique was used to find *SEA* and minimum initial crushing force.

Hussein et al. [127] investigated the crushing performance of four types of tube combinations: A square empty aluminum tube, shown in Fig. 31(a) [127]; an aluminum honeycomb-filled tube, shown in Fig. 31(b) [127]; a polyurethane foam-filled tube, shown in Fig. 31(c) [127]; and an aluminum tube filled with polyurethane and aluminum honeycomb, shown in Fig. 31(d) [127], under quasi-static loading condition. The square aluminum tube filled with polyurethane and aluminum honeycomb performed better in terms of mean crushing force (increased by 349%), energy absorption (increased by 334%), and *SEA* (increased by 109%) compared with the hollow square tube.

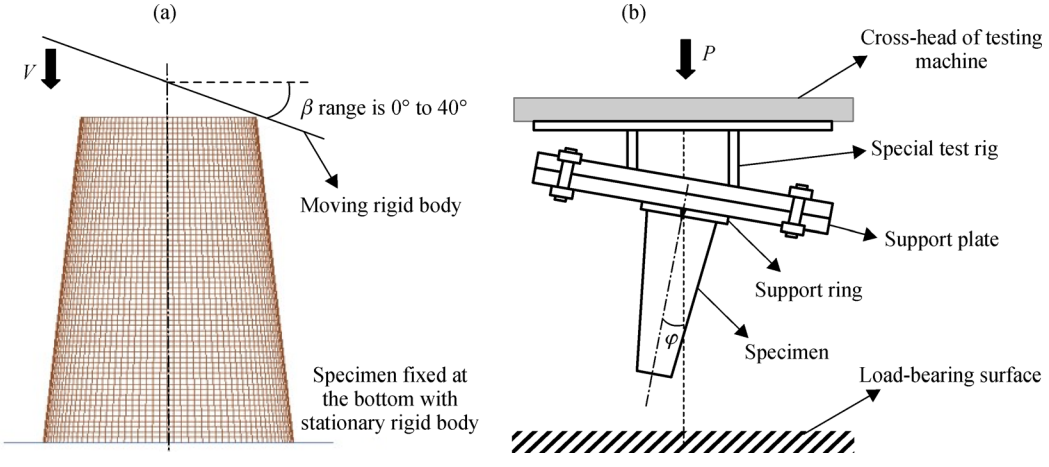

Fig. 28 (a) Finite element model under oblique loading condition and (b) experimental setup for oblique loading. *P*: Applied load. Reproduced with permission from Ref. [122] from Elsevier.

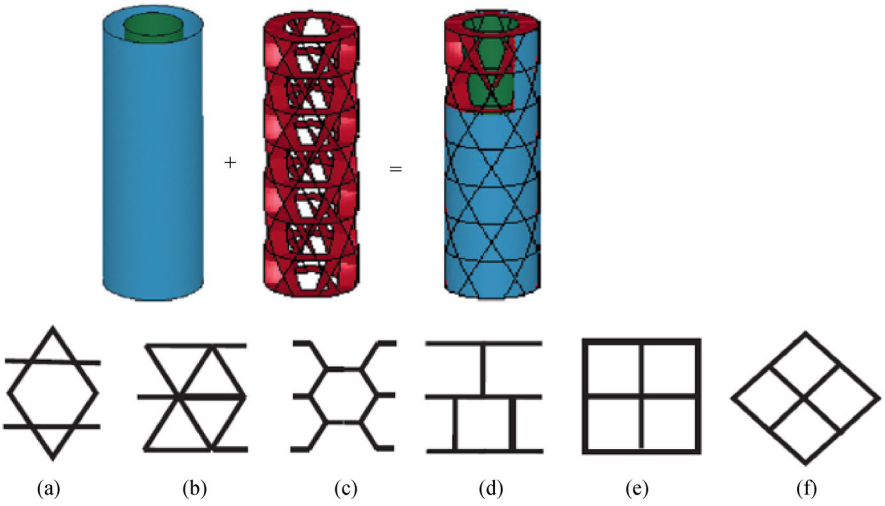

Fig. 29 Geometric configurations of honeycomb sandwich columns: (a) Kagome, (b) triangle, (c) hexagon, (d) square-3, (e) square-4, and (f) diamond. Reprinted with permission from Ref. [125] from Elsevier.

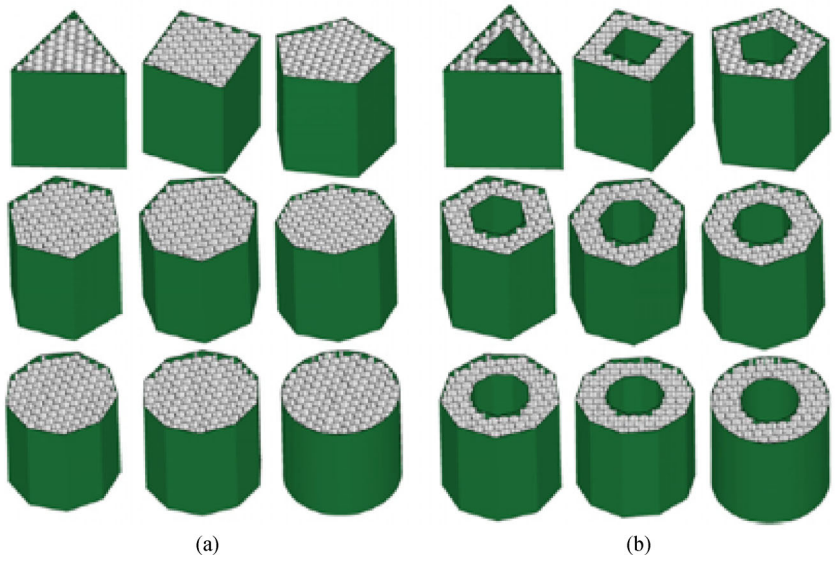

Fig. 30 Configuration of honeycomb-filled single and bi-tubular polygonal tubes ($N = 3$, 4, 5, 6, 7, 8, and ∞): (a) Single polygon tubes and (b) bi-tubular polygon tubes. Reprinted with permission from Ref. [126] from Elsevier.

4.2 Multi-cell tubular structures

The energy absorption capacity of tubular structures is influenced by many factors, such as material, boundary condition, cross section of the structures, and thickness. Among the aforementioned factors, cross-section geometry is one of the important. Therefore, improvement is required in cross sections by incorporating cells into a simple tubular framework. Similar to square and rectangular tubes, polygon tube structures [128,129] have been analyzed numerically to determine their crashworthy performance. Zhang and Huh [130] performed a comparative analysis of different polygon structures ($N = 3$ to $N = 10$, where N represents polygon faces) and observed three types of deformation modes: In-extensional, extensional, and mixed modes. The polygon with even faces presented regular deformation compared with the polygon with odd faces.

Studies on polygon structures have focused on angle plate, i.e., in the form of different cross-sectional tube structures, such as triangle, rectangle, and pentagon. Researchers have designed a new structure in the form of a multi-angle plate called a multi cell tubular structure. Zhang et al. [131] analytically and numerically explored the deformation behavior and energy absorption capability of a square multi cell tubular structure made of aluminum alloy AA-6060 T4 under quasi-static and dynamic loading conditions. Multi-cell tubes were divided into three parts: Corner, shown in Fig. 32(a) [131]; crisscross, shown in Fig. 32(b) [131]; and T-shaped, shown in Fig. 32(c) [131],

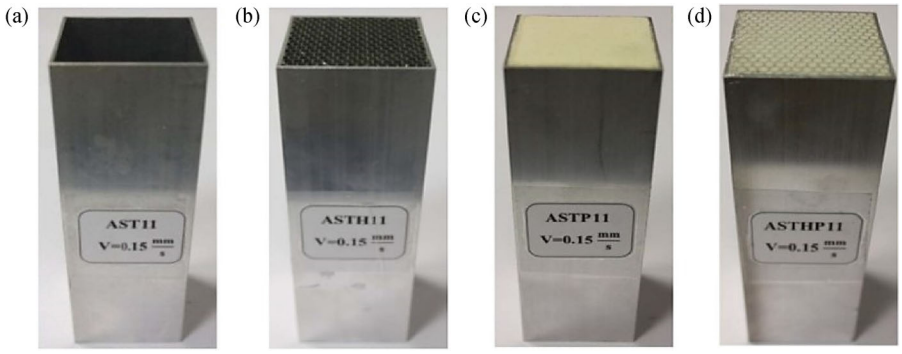

Fig. 31 Prepared samples: (a) Empty square aluminum tube, (b) aluminum honeycomb-filled tube, (c) polyurethane-filled tube, and (d) tube filled with honeycomb and foam. Reprinted with permission from Ref. [127] from Elsevier.

to derive a theoretical model for mean crushing force based on super folding element theory. The crisscross part was efficient as an energy absorber. Energy absorber efficiency increased by 50% for the 3 × 3 cell tube compared with the single-cell column.

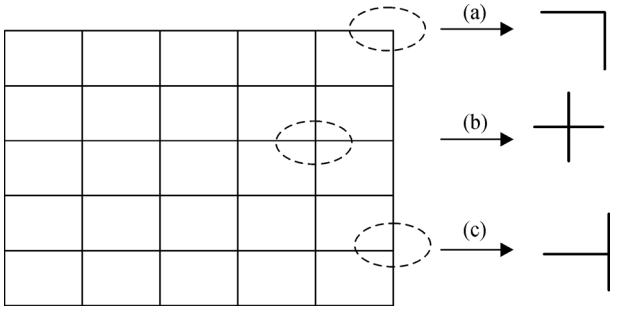

Fig. 32 Division of multi-cell section: (a) Corner, (b) crisscross, and (c) T-shaped. Reprinted with permission from Ref. [131] from Elsevier.

Tran et al. [132] performed theoretical predictions and numerical simulation to optimize the design of an aluminum multi-cell square tube that was tested under dynamic oblique loading. Theoretical analysis was based on the simplified super folding element [133]. Mathematical expressions were derived for mean crushing force, mean horizontal force, and mean bending force by considering different angle elements (right corner, T-shaped, crisscross, 3, 4, 5, and 6 panels) shown in Fig. 33 [132].

The multi-cell tubular structures, shown in Fig. 34(b) [134], with laterally variable thickness [134] were studied experimentally and numerically. Theoretical prediction of energy dissipation and mean crushing force was conducted by considering three angle element parts, namely, corner L-shaped, T-shaped, and crisscross, as shown in Fig. 34(a) [134].

Zhang and Zhang [135] studied the performance of multi-cell columns with different sections (Fig. 35) under axial quasi-static loading and showed that multi-cell columns were more energy efficient than single-cell columns. The numerical analysis results were validated with the experimental results, and a theoretical model for mean crushing load was derived.

Similarly, Tang et al. [136] conducted a numerical simulation of a cylindrical multi-cell tube structure and found that cylindrical multi-cell columns were more efficient in terms of energy absorption than a square column with a single cell or multiple cells. Multi-cell structures were also studied with the use of filler materials to evaluate the effect of filler addition. Yin et al. [137] optimized the crashworthiness performance of six types of foam-filled multi cell aluminum alloy, AA-6060 T4 tubular

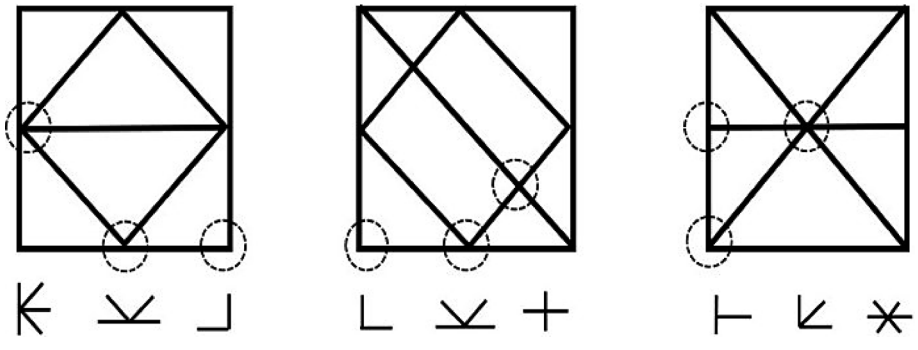

Fig. 33 Multi-cell tube cross section with different angle elements. Reprinted with permission from Ref. [132] from Elsevier.

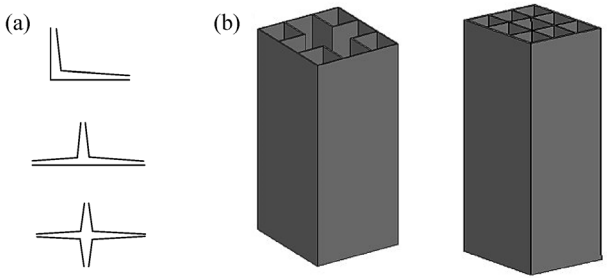

Fig. 34 (a) Angle element with varying cross sections and (b) specimen for axial testing. Reprinted with permission from Ref. [134] from Elsevier.

structures (Fig. 36) [137] with different numbers of cells (n = 1, 2, 3, 4, 6, and 9) by using the nonlinear finite element code LS-DYNA. All the structures were selected for multi-objective particle swarm optimization to obtain the optimum value of *SEA* and the maximum peak collapse force. The foam-filled multi-cell thin-walled structure with nine cells exhibited better crashworthy performance than the other studied foam-filled multi-cell thin-walled structures.

Hong et al. [138] performed a quasi-static axial test on multi-cell tube with two section types: Triangular lattice, shown in Fig. 37(a) [138], and Kagome lattice, shown in Fig. 37(b) [138], structures. The multi-cell tubes demonstrated better ability to absorb energy as they deformed progressively.

Tabacu [139] studied the collapse behavior of an aluminum AA-6061-O circular tube with a multi-cell insert (Fig. 38) under an oblique impact velocity of 5 m/s. A series of simulations was conducted to validate the proposed analytical model for mean crushing force, which was found to be in good agreement with the result obtained in simulations.

4.3 FGT tubular structures

Comprehensive research of thin-walled functionally

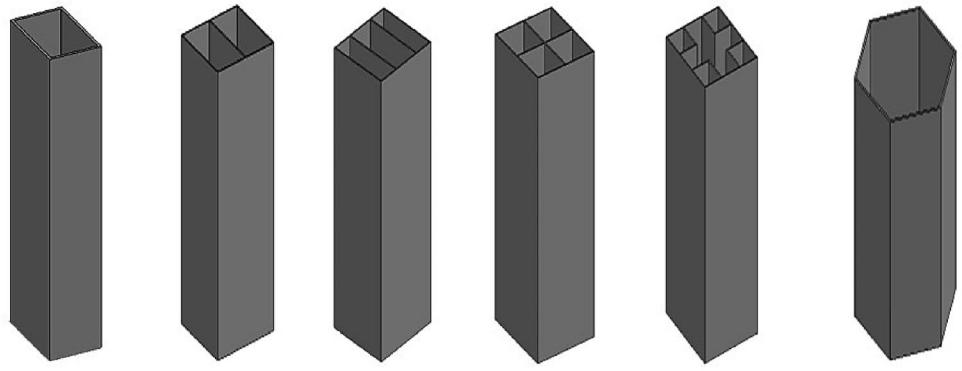

Fig. 35 Multi-cell tube with different sections. Reprinted with permission from Ref. [135] from Elsevier.

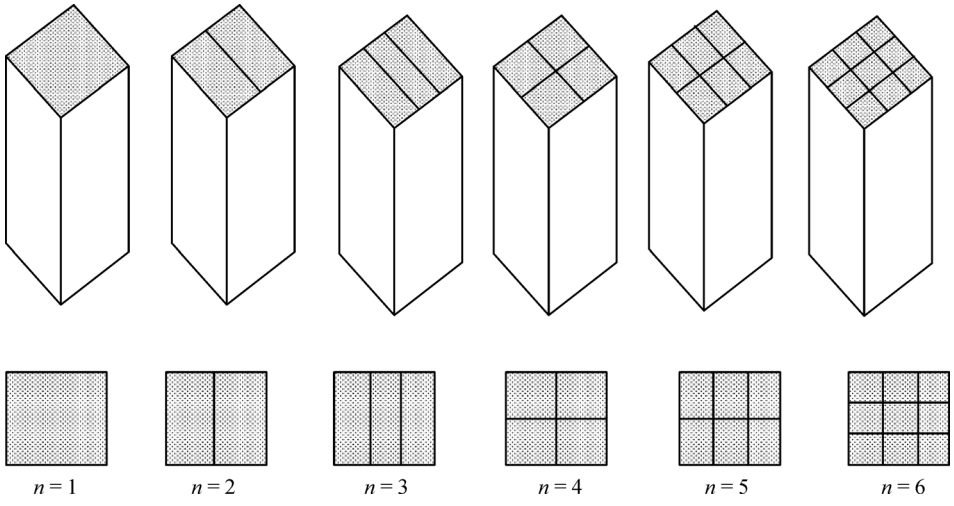

Fig. 36 Schematic representation of foam-filled tubular structures with different cell configurations. Reprinted with permission from Ref. [137] from Elsevier.

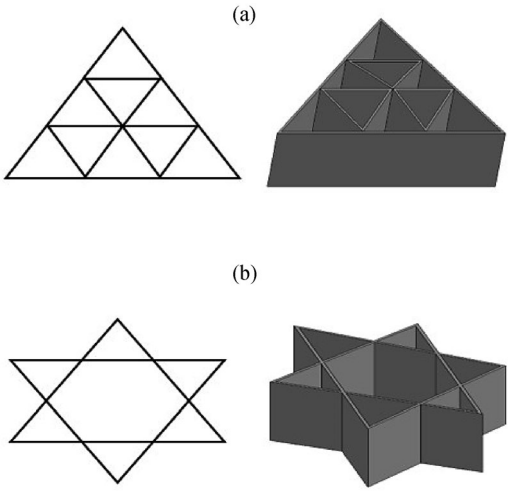

Fig. 37 Multi-cell tubes: (a) Triangular lattice and (b) Kagome lattice. Reprinted with permission from Ref. [138] from Elsevier.

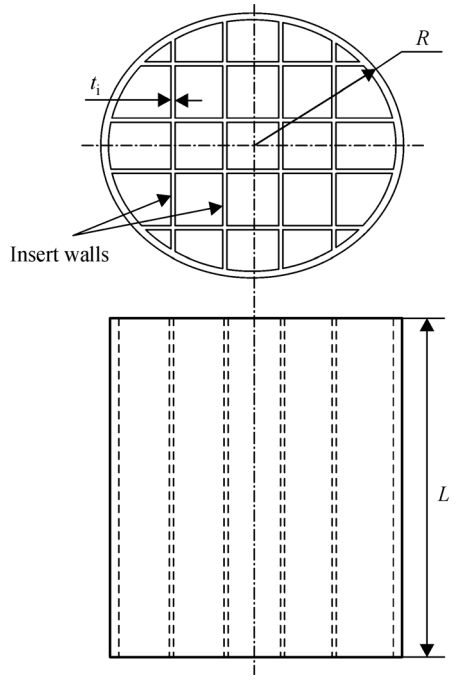

Fig. 38 Schematic of a circular tube with inserts. t_i: Insert wall thickness; R: Radius of shell/tube. Reproduced with permission from Ref. [139] from Elsevier.

graded structures has been performed in recent years. Implementing graded thickness on structures subjected to any loading condition will help to enhance their efficiency to absorb substantial impact energy. The development of structures in terms of FGT provides maximum utilization of materials in accordance with the deformation zone. This approach provides a thin-walled structure that can absorb the maximum amount of impact energy to enhance *SEA*. It also helps to decrease the initial peak load, which is the primary cause of global bending. Different cross-sectional (circular, square, and frusta) thin-walled tubular structures have been developed as FGT to explore crashworthiness performance. Thickness is varied either in the longitudinal direction (for the circular section) to reduce the initial peak at the start of impact [140–143] or in the transverse direction in case of corner-type structures (mostly square cross sections) [144,145] to increase energy absorption efficiency (Fig. 39).

Chirwa [140] first reported the inversion buckling of a circular tapered tube with graded thickness in the longitudinal direction. The energy absorption capacity increased by up to 50% compared with the taper structure with uniform thickness and the same mass. Li et al. [143] performed a comparative study of circular tapered FGT tubes with straight and tapered tubes with uniform thickness under dynamic oblique loading. The study demonstrated that FGT tubes were more reliable than their counterpart's structures with uniform thickness. Gupta [146] reported the effect of nonuniformity of thickness along the height of a tapered tube and explored deformation modes. Apart from thickness nonuniformity, taper angle and $\overline{d}/t$ ratio was also considered for a detailed study of deformation mode. All frusta tubular structures collapsed in the axisymmetric deformation mode. They included initial concertina fold, followed by a plastified zone, where plastic hinge expanded when further compression occurred. Zhang and Zhang [147] investigated the advantage of a conical steel tube with graded thickness (CTGT) under oblique loading condition. The effects of structure layout (Fig. 40 [147]), load angle, inertia, strain rate, and forming on CTGT were analyzed computationally using a finite element model and further validated through experiments.

The tube-shrinking process [148] was used for nonlinear thickness distribution, and the crashworthiness performance of circular frusta was explored. As thickness and material hardening increased during the tube-shrinking process, energy absorption was increased by 120%, even for low mass values. The result of the tube-shrinking process increased the mean force considerably faster than the maximum force, reflecting uniformity in the load–displacement curve with an increase in *CFE*.

Zhang et al. [144] explored square tubes with two types of graded thickness (single surface gradient and double surface gradient) in the transverse direction (Fig. 41 [144]) under axial loading. The mean crushing force of the gradient tubular structures increased by 30%–35% compared with that of a square tube with uniform thickness.

Fang et al. [149] extended the work of Zhang et al. [144] in the form of multi-cell tubes with transverse variable thickness (Fig. 42 [149]) under axial dynamic loading. FGT multi-tubes provided significant increases in *CFE*,

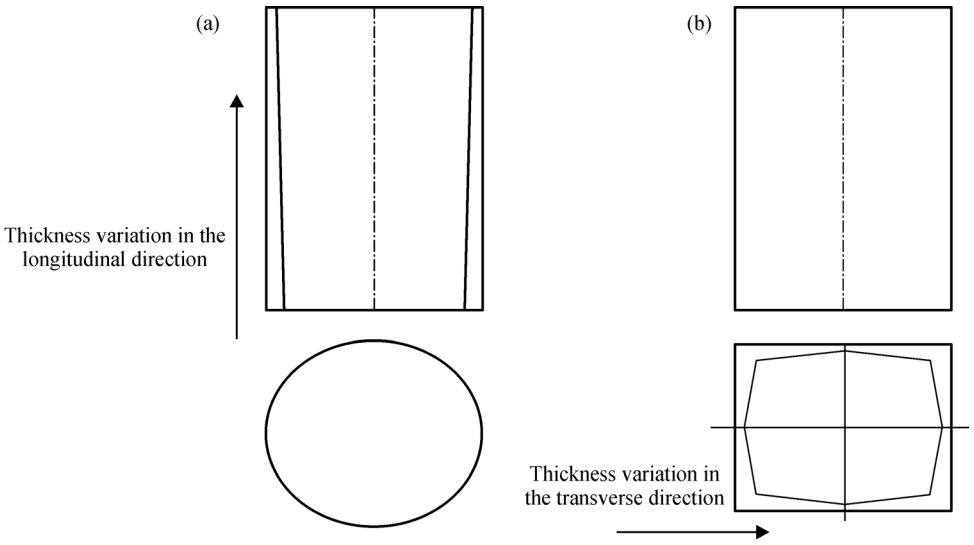

Fig. 39 FGT variation in tubes: (a) Longitudinal direction and (b) transverse direction.

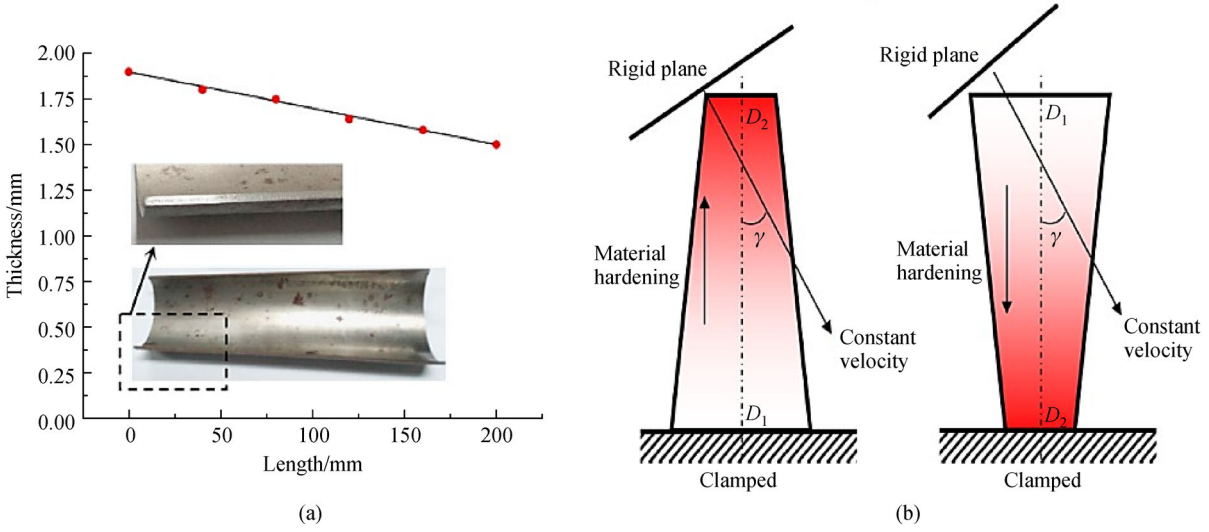

Fig. 40 (a) Thickness nonuniformity and (b) structural layout of CTGTs under oblique load. Reproduced with permission from Ref. [147] from Elsevier.

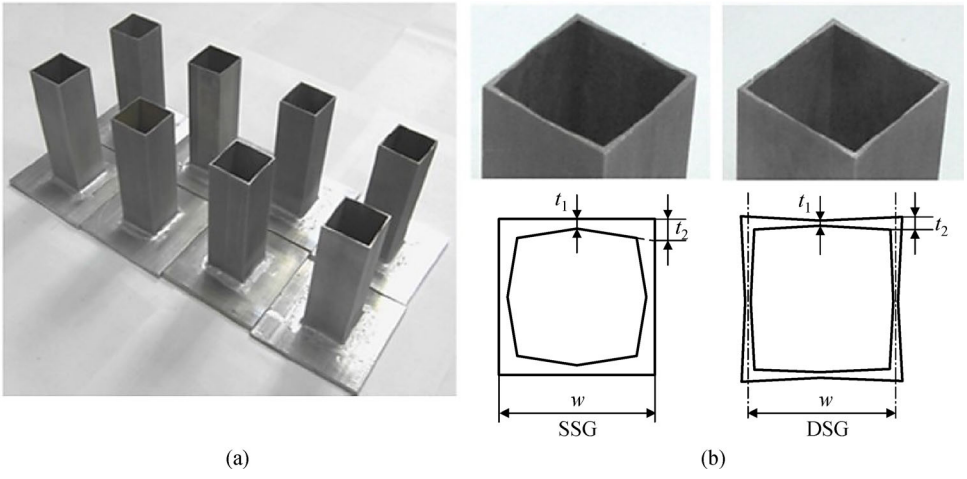

Fig. 41 Prepared specimens: (a) Square tube with uniform and graded thickness and (b) two configurations of graded thickness. Reproduced with permission from Ref. [144] from Elsevier.

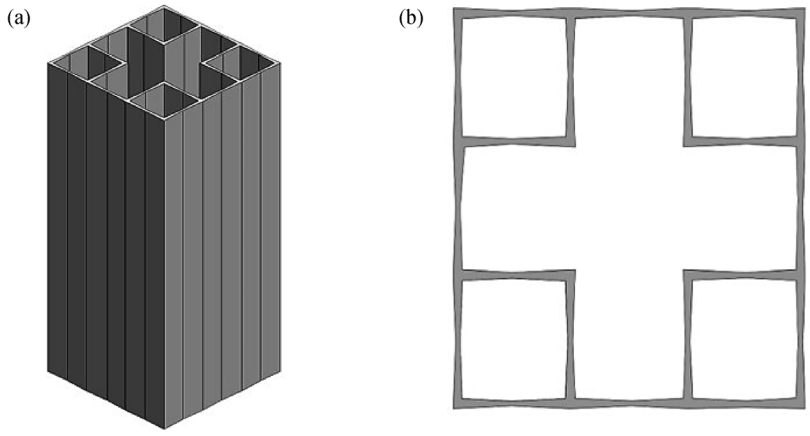

Fig. 42 FGT multi-cell tubes: (a) 3D view and (b) 2D view. Reprinted with permission from Ref. [149] from Elsevier.

EA, and *SEA* compared with a uniform thickness multi-tubular structure.

An optimization design technique with numerical analysis [150] was also adopted to improve the crashworthiness performance of gradient multi-cell tubular structures. The performance of a square tube with longitudinal graded thickness was numerically analyzed, and it performed better than the tube with uniform thickness. Further multi-objective optimization technique was selected to increase *SEA* and minimize initial peak force.

4.4 Multi-tubular structures

These structures are a combination of two or more tubes with different cross sections placed asymmetrically or concentrically.

Haghi Kashani et al. [151] developed a square bi-tubular structure with two arrangements of the inner tube: Parallel and diamond, as shown in Fig. 43. The structures were investigated experimentally and numerically under quasi-static loading to predict the energy absorption capability. The results showed that the bi-tubular arrangement absorbed more energy than the sum of the energy of each tube. Apart from tube arrangement, the authors also focused on the effect of change on height in either the inner or outer tube and concluded that bi-tubular structures performed better when the inner part was shorter.

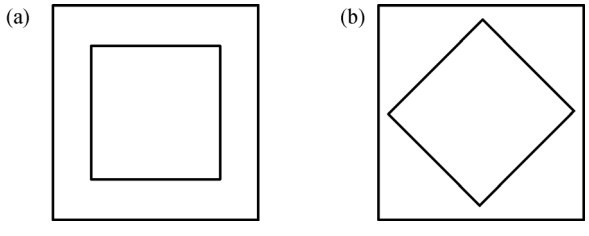

Fig. 43 Configuration of bi-tubular specimens: (a) Parallel and (b) diamond arrangements. Reprinted with permission from Ref. [151] from Elsevier.

Other published literature has emphasized circular bi-tubular structures with variation in inner tube cross section. In this context, Sharifi et al. [152] explored the energy absorption capability of bi-tubular circular structures made of AL-6063-O, placed coaxially, and compressed under quasi-static loading. Interaction effect, thickness, and diameter were considered major deciding parameters to enhance the performance of bi-tubular structures. The authors used two techniques, varying length [151] and creating grooves on the tube surface, to reduce initial peak load. The tight contact between coaxially placed tubes caused high load fluctuations and an irregular collapse mode. Meanwhile, the large distance between tubes caused individual deformation of the tubes.

The performance of bi-tubular and tri-tubular structures for circular and square sections was compared by Goel [153] with the addition of foam filler. The circular section gained more energy than the square section. Foam interaction was also investigated. The variation in the inner part, while keeping the outer part circular, of a bi-tubular structure was studied by Azimi and Asgari [154] under axial and oblique loading conditions. Apart from the configuration of bi-tubular structures, the effect of foam filler was also considered. The obtained results showed that bi-tubular structures were preferable under oblique loading condition. Similarly, Vinayagar and Kumar [31] modified a bi-tubular structure with a fixed outer circular section, while the inner section was changed to triangle, square, and hexagon. Crashing performance was studied by keeping the dimensions of the outer section constant with a variation in the inscribed polygon section. The combination of a circular tube with a hexagonal inner section was a good energy absorber candidate compared with the other combinations.

In addition to the aforementioned studies, the effect of the number of tubes made of AA-6101 and placed coaxially was examined by Nia and Chahardoli [155] under quasi-static axial load. The results implied that *SEA* and *CFE* increased compared with those of a monolithic

structure with the same mass, height, and thickness. The distance between multi-wall tubular structures plays an important role in the overall deformation characteristics. In this context, Estrada et al. [156] discussed the crushing behavior of circular, square, and hexagonal bi-tubular structures in terms of radial clearance with cutouts as crush initiators.

4.5 Hierarchical and self-locking energy absorbers

In addition to filled tubes, multi-cell and multi-wall tubular structures, a new hierarchical lattice structure has been explored in the published literature [157–161]. This structure is a combined form of multi-cell and filler to develop different cross-sectional hierarchical energy-absorbing components. Sun et al. [157] adopted the effectiveness of hierarchical lattice sandwich walls as core to increase the anti-crushing performance of a triangular structure. The authors explored the folding mechanism of hierarchical structures that helped enhance anti-crushing characteristics. A theoretical expression for mean crushing force ($\overline{F}$) was derived based on this fold mechanism. The performance of the proposed structure was compared with those of single-cell and multi-cell structures and found that $\overline{F}$ was improved 3–4 times. Another study by Sun et al. [158] examined the effect of in-plane crushing on the same hierarchical structures. The structure did not improve yield strength but helped resist the buckling of cellular structures.

Luo and Fan [159] numerically and analytically studied the energy absorption capability of rectangular sandwich walled tubes (SWTs) made of AA-6061-O. The authors compared the SWT structure with a square tube with the same mass. The SWT absorbed more energy because it restricted the bending that appeared in conventional tubes of the same wavelength. The multi-cell structure formed a number of lobes during crushing that helped absorb substantial impact energy. Theoretical analysis was also proposed on the basis of the folding mechanism. In the same context, Li et al. [160] investigated the performance of a hierarchical tubes (HT) in the form of hexagonal multi-cell through experiment, simulation, and theoretical prediction. The specific energy absorption of HT was two times that of a single cell tube.

The authors found that three forms of folding (sub-cell, global, and mixed mode folding) appeared during the crushing of HT. Theoretical analysis was performed on the basis of such folding mechanism to compare experimental and numerical findings. Fan et al. [161] performed experimental, numerical, and analytical studies on the higher order of a hierarchical rectangular tubular structure. During deformation, three folding mechanisms defined absorber performance. With additional hierarchical orders, the $\overline{F}$ of structures reached its full intensity in plastic strength.

Tubular structures under lateral loading are ineffective for absorbing the maximum amount of impact energy. Therefore, the design and shape of structures should be improved to enhance crashworthiness properties under lateral loading. In this regard, Chen et al. [162] proposed a novel self-locked energy-absorbing structure with dumbbell shape (Fig. 44) made of mild steel that interlocked to provide lateral constraint during compression. The authors discussed the shape and stacking arrangement of the dumbbell-shaped structure that helped prevent the splashing of the tube, which occurred in the case of a circular tube with the same arrangement.

Yang et al. [163] discussed the effect of lateral dynamic

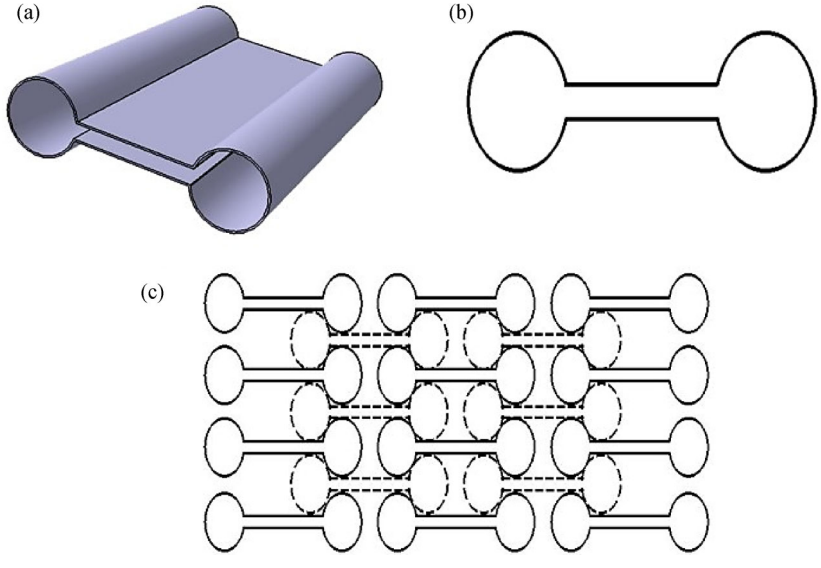

Fig. 44 Schematic of the (a) dumbbell-shaped novel tube, (b) cross-sectional view, and (c) self-locking tube. Reprinted with permission from Ref. [162] from Elsevier.

impact loading on the deformation characteristics of 201-stainless steel self-locking tube structures. At low impact velocity, the authors found four stages of deformation (shock wave progression, energy conversion, densification, and bounce back); as velocity increased, they changed into three stages of deformation (global compression, compression followed by crushing, and progressive crushing). Yang et al. [164] suggested that the structure proposed in Refs. [162,163] did not fully utilize the capability of tubes to absorb impact energy. Thus, the structure was redesigned with the enclosed and unenclosed forms of a self-locking energy absorber. Eight types of self-locking structure were explored under quasi-static loading (Fig. 45 [164]). The unenclosed structure exhibited higher stability under compression, but the enclosed structure provided better load-carrying capacity.

The nested tubular structures are easier to design compared to the multi-cell with structures. Thus, many researchers [165–169] have explored the performance of a stacked tube to determine the potential of such system to absorb impact energy. Stacked or nested systems are designed for specific applications with a limited stroke length. A nested tube has a number of energy-absorbing systems in the same space, showing its ability to absorb maximum impact energy per unit length compared with a single tube [165]. A parametric study was performed by Baroutaji et al. [165] to investigate the performance of a nested tubular structure under lateral quasi-static and dynamic loadings. Three types of nested tube structures (Fig. 46 [165]) that consisted of circular and oblong tubes were studied. Under low-velocity impact, strain rate had no significant effect. Under quasi-static and dynamic loadings, the response of the force–displacement curve was the same.

Olabi et al. [166,167] performed experimental and numerical analyses on oblong and circular nested tube systems to demonstrate the effect of constraints. The crushing behavior of a nested tube was improved with the use of constraint in the form of a circular rod. Wang et al. [168] explored the response of a nested tube system through experiment, simulation, and theoretical analysis against lateral impact. The theoretical solution was derived by considering the effects of strain hardening and strain rate. Tarlochan and Ramesh [169] developed a composite sandwich tubular structure in the form of a nested insert and analyzed it under axial quasi-static loading. The results were compared with those of metallic (aluminum and steel) counterparts and good potential was demonstrated in terms of crashworthiness performance.

5 Discussion

Simple tubular structures were studied with reference to geometry (uniform structures, such as circular, rectangular, and square, along with nonuniform structures, such as conical and rectangular/square frusta), selected material (steel, aluminum, and composite), and loading axis (axial

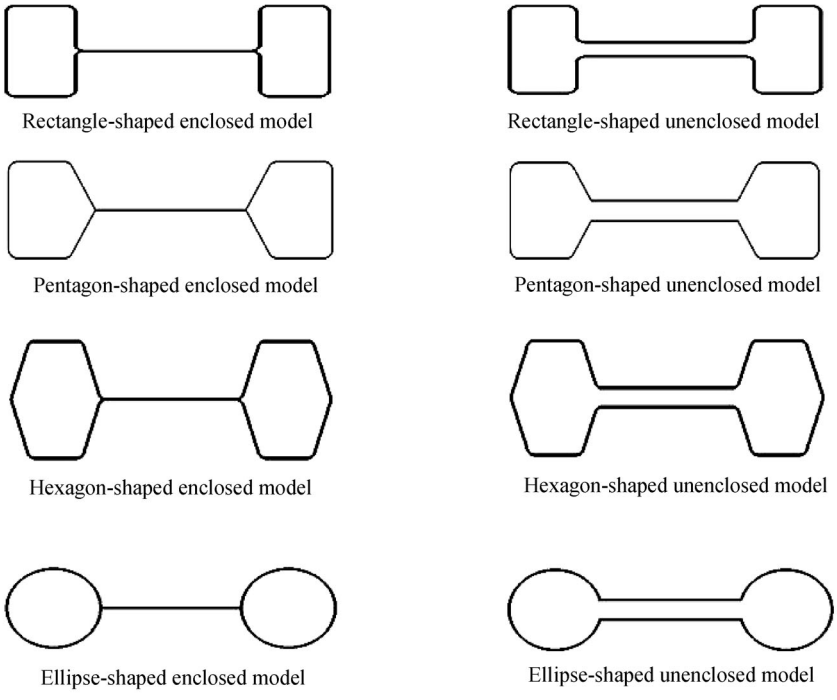

Fig. 45 Self-locking energy absorber with enclosed and unenclosed forms. Reproduced with permission from Ref. [164] from Elsevier.

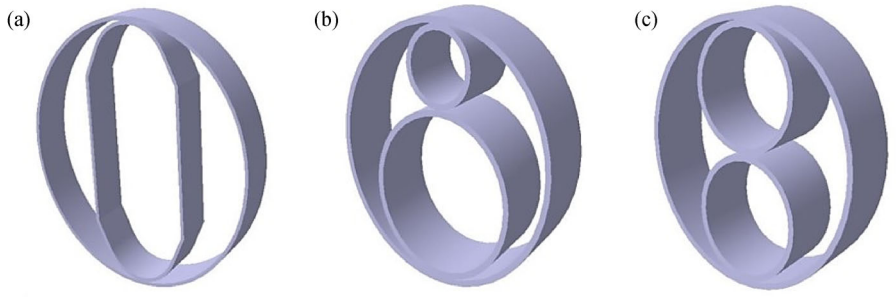

Fig. 46 Nested tubular structures incorporating the same outer circular part with different inner parts such as: (a) An oblong cross-section, (b) two circular tubes of different diameters, and (c) two circular tubes of the same diameter. Reprinted with permission from Ref. [165] from Elsevier.

and oblique) with quasi-static and dynamic impacts. The effects of multi-cell and foam-filled structures also focused on crashworthiness performance. Important observations were made on the basis of obtained failure modes, the response of the load–displacement curve, and crashworthiness parameters, such as $F_{\max}$, $\overline{F}$, *CFE*, E_{ab}, and *SEA*.

5.1 Failure modes

The important factor for a structure at the moment of crash is how it absorbs energy from impact by deforming itself. The characteristics of structure deformation predict its ability, i.e., the structure may or may not be appropriate for a certain application. The studied literature mentioned different failure modes, such as concertina or axis-symmetric, diamond, Euler buckling, a mix of both concertina and diamond, splitting, and tearing [44,45, 170]. Splitting and tearing occur when constraint motion exists to absorb energy, which is unlikely in conventional collapse. In case of splitting and tearing, impact energy loss is initially absorbed in the form of friction energy; after tearing, energy loss occurs, leading to further progressive collapse, such as in conventional structures without any constraint. These failure modes are generally evident in a square section because such section has corner elements. The diamond and mix mode occur mostly when large deformation exists [18], leading to the possibility of Euler buckling [171] for uniform tube structures. In large structures, Euler buckling must be avoided because of their low energy absorption at the time of impact due to the lateral inertia effect. A tapered section was selected; different failure aspects were analyzed; and frusta tube response was good, even for long tubes [76], which can replace the uniform section at the same level. The corrugation or grooves on the surface of tubular structures is another means to reduce the bending mode of failure. It helps to deform a structure in a controlled manner and form concertina mode that is a considerable choice for high performance under impact condition [23–25,32,33]. Providing cutouts minimizes the chances of Euler buckling deformation mode. Material behavior is also a dominant factor for selecting the characteristic of the deformation pattern. The annealed condition for steel collapses in diamond mode, and the non-annealed condition follows concertina mode; for aluminum, modes are obtained in reverse pattern [22]. Failure patterns are affected by the addition of a cellular type of structure, such as foam or honeycomb. With the addition of such structure, the diamond mode changes to the axis-symmetric mode of deformation [111].

5.2 Load–compression curve

A curve represents the dissipation of impact load when a collapse happens. In case of conventional uniform structures, a load drops at a low value after it fluctuates continuously upon reaching the maximum initial peak. The load–displacement curve behavior should be smooth [66] as the structures deform, reflecting efficient functioning under the event of a crash. The initial maximum force is considered an important factor in the design phase of an energy absorber that is associated with safety. It should be kept under a certain limit rather than at the maximum value because it is desirable at the time of impact. This behavior can be easily predicted by simply observing the response of the load–displacement curve.

The response of a multi-cell tubular structure was compared with that of a single-cell structure, and similar deformation characteristics, shown in Fig. 47(a) [172], were found, except for the change in initial maximum force. In the foam-filled multi-cell tubes shown in Fig. 47(b) [172], load increases as collapse progresses. This phenomenon happens as deformation progresses to the densification of foam, and interaction with the structure leads to an increase in load.

The deformation response of a tapered tube filled with foam is affected by wall thickness but not by taper angle [121,173]. Deformation must begin at an early stage of the impact for a smooth curve flow, which maintains a steady fluctuation in a significant limit of the mean load.

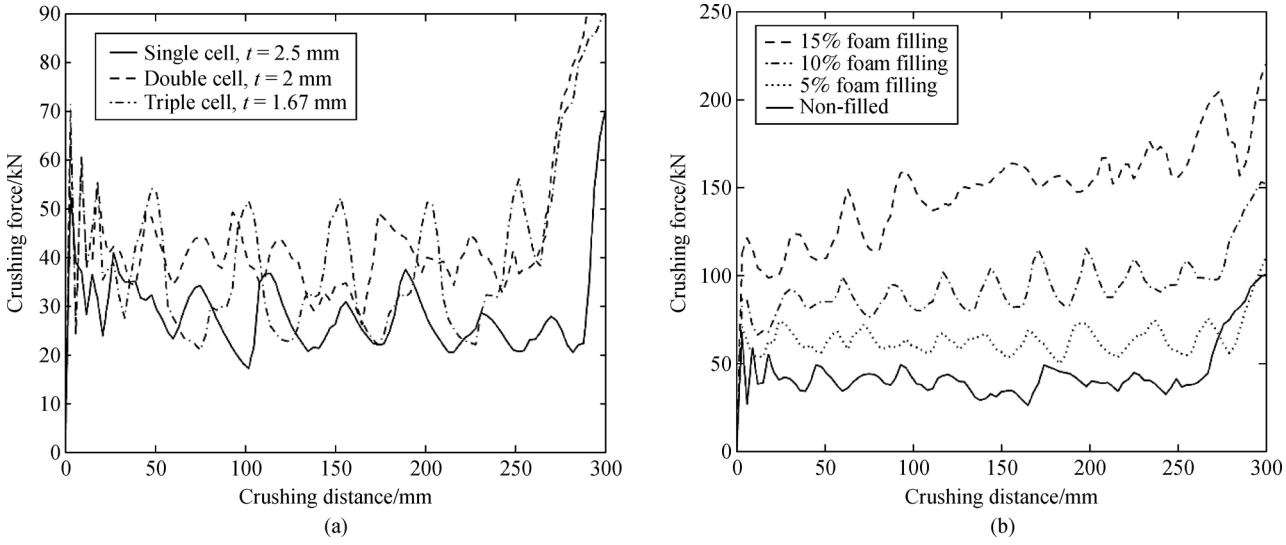

Fig. 47 Comparison of the load–displacement plots of multi-cell tubular structures: (a) Without foam and (b) foam-filled. Reproduced with permission from Ref. [172] from Elsevier.

5.3 Crushing efficiencies

A comparative study of different cross sections (circular, square, rectangular, hexagon, triangular, pyramidal, and conical) showed that the *SEA* of a cylindrical tube was the maximum, whereas the difference in F_{max} and $\overline{F}$ was the minimum for a frusta tube [174]. The initial peak should be minimum to avoid a large reaction force, which is felt by the adjacent object, whose safety is important. The use of cutouts in tubular structures minimizes initial peak force, helping initiate deformation at low loads.

An increase in the number of grooves decreases initial peak force and follows a progressive deformation that provides stability to the structure and improvement in mean crushing force [23]. Corrugation direction is a deciding factor for a good energy absorber. Two types of corrugation, radial and lateral, have been studied. E_{ab} is enhanced with radial corrugation. Cutout sections, mostly circular and elliptical cutouts, were provided to structures to reduce the initial peak force that acts as a trigger. With an increase in the major axis of elliptical cutouts, uncontrolled folding occurs, decreasing the E_{ab} of structures [29]. Initial peak force can be controlled by providing constraint deformation in the form of capped and uncapped structures. It was reduced by 15%–30% when capped tubes were used in place of uncapped tubes, but no considerable variation in E_{ab} occurred [36,37]. In case of a frusta tube, an increase in $t/\overline{d}$ ratio increases maximum force and mean force; an increase in semi-apical angle decreases maximum force [65].

Structures filled with cellular solids, such as foam or honeycomb, have attracted designers because they have higher absorption capacity than empty structures. *SEA* was increased by 30% for a single cell filled with foam and 40% for double and triple cells filled with foam compared with a non-filled structure [172]. The honeycomb filler is not as effective as the foam filler because it resists only unidirectional impact force and does not consider the combined effects of compression and bending [123]. Foam density plays an important role, given that an increase in density results in a dense region that increases $\overline{F}$. Densification decreases folded length to prevent the possibility of Euler buckling mode. A comparison of a foam-filled single-cell structure with a multi-cell structure presented 50%–100% increase in the E_{ab} of the multi-cell tube, indicating that the multi-cell structure is a better choice than the foam-filled tubular structure [175]. The multi-cell structure depends on the angle element that determines the ability of the structure to absorb energy. The angle elements used are mostly T-shaped, L-shaped, and crisscross with uniform thickness and gradually varying thickness [134].

6 Future guidance

The primary objective of researchers is to develop a lightweight component that exhibits good crashworthiness performance during a crash scenario. To achieve this objective, several points, such as material behavior, absorber cross section, and loading condition should be appropriately examined. In this review paper, aluminum alloy, steel, and composite materials are explored in detail. Aluminum alloy is dominant over the other materials for the same area of crashworthiness. Further research on lightweight composite materials must be performed to define them as promising candidates in the field of energy-absorbing components.

Among all conventional tubular components, tapered tube exhibits better performance against oblique loading

impact. Tapered structures with circular and square/rectangular sections are extensively focused on by researchers. Other possible polygon sections should be added to future work to explore performance under the same loading condition.

Advanced tubular components derived from conventional structures exhibit good performance under axial loading, but studies on the response of structures under lateral loading condition remain highly limited. In this context, studies on nested tubular structures that exhibit high crashworthiness performance are also limited. These structures should be explored further to predict their performance and deformation behavior under lateral loading.

The performance of cellular materials used as fillers exerts considerable impact on crashworthiness performance. Cellular structures, namely, honeycomb and foam, are investigated in this study under static and dynamic loadings. The analysis of components filled with foam is difficult because it relates to the microstructure, which must be properly understood during the loading process. Mathematical models that incorporate such complexity and provide a deep understanding of the crushing response of foam-filled structures have been developed by researchers. These models should be included in the future to discuss the crashworthiness performance of energy absorbers under dynamic loading.

7 Summary

Mechanical behavior, energy absorption, and collapse mode are essential to study when developing or designing a tubular structure. Tubular structures with different cross sections have been studied in the published literature with variations in geometric parameters (slenderness ratio, tube length, tapered angle for tapered tube, multi-cell, and thickness throughout the length). Loading parameters (impact condition, either quasi-static or dynamic, and load angle for oblique loading) have also been considered important prospects for deformation behavior. Foam- and honeycomb-filled cellular structures provide desirable output related to crashworthiness performance. From the experimental and numerical outcomes of several papers, the important factors used for the efficient functioning of energy absorbers are as follows.

• The slenderness ratio and length of tubes are major factors that determine their deformation characteristics and affect the performance of energy absorbers. As slenderness ratio increases, $F_{\max}$ and $\overline{F}$ also increase; as length increases, structures will fail via bending, which reduces E_{ab}.

• Corrugation on tubular structures reduce the chances of Euler buckling and helps deform structures in a progressive manner with the formation of concertina mode. The direction of corrugation determines the performance of collapsible structures. When providing radial corrugation, structures deform in concertina mode, which enhances E_{ab}; lateral corrugation increases initial peak, which is undesirable.

• A trigger mechanism helps initiate crushing while reducing initial $F_{\max}$. It is mostly created near the loaded end.

• The deformation characteristic and energy absorption of frusta tubes are primarily affected by a semi-apical angle.

• The bending failure of long tubes can be controlled by creating a slot on structure's surface. Hole diameter and position are key parameters that determine the deformation behavior of collapsible structures.

• In case of foam-filled structures, density is a significant variable that affects crushing response under impact loading. Given that they become dense during collapse, the chances of buckling are reduced, and the possibility of non-axis-symmetric mode changes to axis-symmetric mode. Honeycomb-filled structures provide unidirectional strength, and thus, are unsuitable for applications in which compression and bending simultaneously occur.

• In a multi-cell structure, the circular section provides better results compared with the other sections.

The key component of energy absorbers is a tubular structure that can be in a different form depending on the basis of application. The structures should be properly designed based on available studies and their failure modes. For example, circular structures exhibit good capability to absorb impact energy but deform in Euler buckling mode while collapsing under oblique loading. Material selection also plays an important role. Circular tubes made of aluminum and steel have different capabilities to absorb impact energy. The difference is due to the rupture strain of materials. A high value (for steel) leads to improper use of the available materials to absorb energy. A low value (for aluminum alloy) indicates a sufficient amount of energy absorbed under static and dynamic loadings. Extensive literature on collapsible structures has concluded that effective points are related to deciding parameters for a desirable output that will assist in designing a structure with excellent crashworthy properties. These points are as follows.

• For a good energy absorber, the structure should not only depend on energy absorption capability but also on other factors, such as smooth graph, high *CFE*, and minimal difference in $F_{\max}$ and $\overline{F}$.

• Circular tubular structures have good crashworthy properties in uniform section compared with other sections for short stroke or deformation. Frustum tubes exhibit good performance even for long strokes. Therefore, the choice of collapsible structures should depend on the application.

• The combination of conventional tubular and

multicellular (honeycomb or foam) structures shows good capability to absorb impact energy irrespective of the high cost of fabrication.

• Geometric modifications, such as multi-cell and gradually varied thickness or FGT structures, are extensively focused on, and crashworthiness response is studied. Both modifications in structure have different objectives to participate in crushing behavior. Multicellular structures are used to improve energy absorption with the utilization of a number of cells and angle elements. The use of FGT structures is to adopt materials in accordance with deformation location. Locations with severe deformations require a large material zone (thick part of FGT structures) while reducing the amount of materials for a less significant part of the structures.

• Apart from changing the shape of thin-walled structures, using filler in the form of foam or honeycomb in tubular structures is a better approach for improving energy absorption capability. The interaction effect between the tube and the filler material, along with the individual deformation characteristics, leads to absorbing substantial impact energy.

• The interaction among tubes in multiwall tubular structures provide better crushing response compared with a monolithic tubular structure. It improves the structure's ability to absorb the maximum amount of impact energy because the maximum amount of materials is involved during collapse.

Nomenclature

F_{max}	Peak force
$\overline{F}$	Mean crushing force
E_{ab}	Energy absorption capacity
SEA	Specific energy absorption
CFE	Crash force efficiency
SE	Stroke efficiency
m	Mass of component
h	Crushed height
L, L_1, L_2	Original height of shell/tube
Y	Yield strength of material
t	Thickness of shell/tube
H	Length of rings between grooves
b	Width of grooves
l	Groove distance
d	Depth of groove
D	Diameter of shell/tube
P	Applied load
b	Load angle
V	Velocity of striker
d_s	Slot diameter
φ	Taper angle of frusta
x	Length between two straight hinges
F_o	End load that causes yielding
R	Radius of shell/tube
w	Width of shell/tube
η	Dimensionless number
$\overline{D}$	Mean diameter of shell/tube
$\overline{d}$	Mean diameter of conical/frusta tube
$\overline{R}$	Mean radius of circular column
K	Constant
θ	Rotation angle
F_a^f	Average crushing force for foam-filled structure
σ_p	Plateau stress
C_a	Dimensionless term for interaction effect
σ_o	Extruded wall stress
R_o	Outer radius of tube
R_i	Inner radius of tube
t_i	Insert wall thickness
D_s	Smaller end diameter of frusta
D_l	Larger end diameter of frusta
t_1, t_2	Gradient thickness
I_1, I_3	Constant integral value in Eq. (5) that depends on cross section
$2N$	Initial distance between the plastic hinges of a folding element
α, γ	Angle defined in Fig. 3
P_o	$Yt^2/4$
E_1, E_2, E_3, E_4, E_5	Energy absorption associated with crushing
r_t	Radius of toroidal shell element
s	Apex height
D_o	Outer diameter of tube
D_i	Inner diameter of tube
d_o	Outer diameter of expanding ring
d_i	Inner diameter of expanding ring
p, q	Side of pyramidal element

Acknowledgements This study was partially supported by SERB/DST under project number DST/SERB ECR/2016/001440 for providing resources. We thank our colleagues from Visvesvaraya National Institute of Technology, India who provided insight and expertise that greatly assisted the research.

References

1. Hanssen A G, Langseth M, Hopperstad O S. Static and dynamic crushing of circular aluminium extrusions with aluminium foam filler. International Journal of Impact Engineering, 2000, 24(5): 475–507
2. Baroutaji A, Sajjia M, Olabi A G. On the crashworthiness

performance of thin-walled energy absorbers: Recent advances and future developments. Thin-Walled Structures, 2017, 118: 137–163
3. Livermore Software Technology Corporation. LS-DYNA Keyword User's Manual. 2007
4. Clausen A H, Hopperstad O S, Langseth M. Sensitivity of model parameters in stretch bending of aluminium extrusions. International Journal of Mechanical Sciences, 2001, 43(2): 427–453
5. Tarigopula V, Langseth M, Hopperstad O S, et al. Axial crushing of thin-walled high-strength steel sections. International Journal of Impact Engineering, 2006, 32(5): 847–882
6. Abramowicz W, Jones N. Dynamic axial crushing of square tubes. International Journal of Impact Engineering, 1984, 2(2): 179–208
7. Abramowicz W, Jones N. Dynamic progressive buckling of circular and square tubes. International Journal of Impact Engineering, 1986, 4(4): 243–270
8. Alexander J. An approximate analysis of the collapse of thin cylindrical shells under axial loading. Quarterly Journal of Mechanics and Applied Mathematics, 1960, 13(1): 10–15
9. Abramowicz W, Jones N. Dynamic axial crushing of circular tubes. International Journal of Impact Engineering, 1984, 2(3): 263–281
10. Hong W, Jin F, Zhou J, et al. Quasi-static axial compression of triangular steel tubes. Thin-Walled Structures, 2013, 62: 10–17
11. Wierzbicki T, Abramowicz W. On the crushing mechanics of thin-walled structures. Journal of Applied Mechanics, 1983, 50(4a): 727–734
12. Abramowicz W, Wierzbicki T. Axial crushing of multi corner sheet metal columns. Journal of Applied Mechanics, 1989, 56(1): 113–120
13. Sun F, Fan H. Inward-contracted folding element for thin-walled triangular tubes. Journal of Constructional Steel Research, 2017, 130: 131–137
14. Jones N. Energy-absorbing effectiveness factor. International Journal of Impact Engineering, 2010, 37(6): 754–765
15. Luo X, Xu J, Zhu J, et al. A new method to investigate the energy absorption characteristics of thin-walled metal circular tube using finite element analysis. Thin-Walled Structures, 2015, 95: 24–30
16. Abramowicz W, Jones N. Transition from initial global bending to progressive buckling of tubes loaded statically and dynamically. International Journal of Impact Engineering, 1997, 19(5–6): 415–437
17. Moalem D, Sideman S. Theoretical analysis of a horizontal condenser–evaporator tube. International Journal of Heat and Mass Transfer, 1976, 19(3): 259–270
18. Pugsley A. The large-scale crumpling of thin cylindrical columns. Quarterly Journal of Mechanics and Applied Mathematics, 1960, 13(1): 1–9
19. Wierzbicki T, Bhat S U, Abramowicz W, et al. Alexander revisited—A two folding elements model of progressive crushing of tubes. International Journal of Solids and Structures, 1992, 29 (24): 3269–3288
20. Singace A A, Elsobky H, Reddy T Y. On the eccentricity factor in the progressive crushing of tubes. International Journal of Solids and Structures, 1995, 32(24): 3589–3602
21. Gupta N, Gupta S. Effect of annealing, size and cut-outs on axial collapse behavior of circular tubes. International Journal of Mechanical Sciences, 1993, 35(7): 597–613
22. Gupta N. Some aspects of axial collapse of cylindrical thin-walled tubes. Thin-Walled Structures, 1998, 32(1–3): 111–126
23. Daneshi G, Hosseinipour S. Elastic–plastic theory for initial buckling load of thin-walled grooved tubes under axial compression. Journal of Materials Processing Technology, 2002, 125–126: 826–832
24. Daneshi G, Hosseinipour S. Grooves effect on crashworthiness characteristics of thin-walled tubes under axial compression. Materials & Design, 2002, 23(7): 611–617
25. Mokhtarnezhad F, Salehghaffari S, Tajdari M. Improving the crashworthiness characteristics of cylindrical tubes subjected to axial compression by cutting wide grooves from their outer surface. International Journal of Crashworthiness, 2009, 14(6): 601–611
26. Karagiozova D, Jones N. Dynamic effects on buckling and energy absorption of cylindrical shells under axial impact. Thin-Walled Structures, 2001, 39(7): 583–610
27. Wang B, Lu G. Mushrooming of circular tubes under dynamic axial loading. Thin-Walled Structures, 2002, 40(2): 167–182
28. Tabiei A, Nilakantan G. Axial crushing of tubes as an energy dissipating mechanism for the reduction of acceleration induced injuries from mine blasts underneath infantry vehicles. International Journal of Impact Engineering, 2009, 36(5): 729–736
29. Huang M, Tai Y, Hu H. Dynamic crushing characteristics of high strength steel cylinders with elliptical geometric discontinuities. Theoretical and Applied Fracture Mechanics, 2010, 54(1): 44–53
30. Isaac C W, Oluwole O. Energy absorption improvement of circular tubes with externally press-fitted ring around tube surface subjected under axial and oblique impact loading. Thin-Walled Structures, 2016, 109: 352–366
31. Vinayagar K, Kumar A S. Crashworthiness analysis of double section bi-tubular thin-walled structures. Thin-Walled Structures, 2017, 112: 184–193
32. Chen D, Ozaki S. Numerical study of axially crushed cylindrical tubes with corrugated surface. Thin-Walled Structures, 2009, 47(11): 1387–1396
33. Eyvazian A, Habibi M K, Hamouda A M, et al. Axial crushing behavior and energy absorption efficiency of corrugated tubes. Materials & Design (1980–2015), 2014, 54: 1028–1038
34. Salehghaffari S, Tajdari M, Panahi M, et al. Attempts to improve energy absorption characteristics of circular metal tubes subjected to axial loading. Thin-Walled Structures, 2010, 48(6): 379–390
35. Nia A A, Khodabakhsh H. The effect of radial distance of concentric thin-walled tubes on their energy absorption capability under axial dynamic and quasi-static loading. Thin-Walled Structures, 2015, 93: 188–197
36. Ghamarian A, Abadi M T. Axial crushing analysis of end-capped circular tubes. Thin-Walled Structures, 2011, 49(6): 743–752
37. Kumar A P, Mohamed M N, Jusuf A, et al. Axial crash performance of press formed open and end-capped cylindrical tubes—A comparative analysis. Thin-Walled Structures, 2018, 124: 468–488
38. Airoldi A, Janszen G. A design solution for a crashworthy landing

gear with a new triggering mechanism for the plastic collapse of metallic tubes. Aerospace Science and Technology, 2005, 9(5): 445–455
39. Zhang X, Tian Q, Yu T. Axial crushing of circular tubes with buckling initiators. Thin-Walled Structures, 2009, 47(6–7): 788–797
40. Liu Y, Day M L. Bending collapse of thin-walled circular tubes and computational application. Thin-Walled Structures, 2008, 46(4): 442–450
41. Zhan Z, Hu W, Meng Q, et al. Continuum damage mechanics-based approach to the fatigue life prediction for 7050-T7451 aluminium alloy with impact pit. International Journal of Damage Mechanics, 2016, 25(7): 943–966
42. Galib D A, Limam A. Experimental and numerical investigation of static and dynamic axial crushing of circular aluminium tubes. Thin-Walled Structures, 2004, 42(8): 1103–1137
43. Yamashita M, Kenmotsu H, Hattori T. Dynamic axial compression of aluminium hollow tubes with hat cross-section and buckling initiator using inertia force during impact. Thin-Walled Structures, 2012, 50(1): 37–44
44. Lu G, Ong L, Wang B, et al. An experimental study on tearing energy in splitting square metal tubes. International Journal of Mechanical Sciences, 1994, 36(12): 1087–1097
45. Huang X, Lu G, Yu T X. Energy absorption in splitting square metal tubes. Thin-Walled Structures, 2002, 40(2): 153–165
46. Han D, Park S. Collapse behavior of square thin-walled columns subjected to oblique loads. Thin-Walled Structures, 1999, 35(3): 167–184
47. DiPaolo B, Monteiro P, Gronsky R. Quasi-static axial crush response of a thin-wall, stainless steel box component. International Journal of Solids and Structures, 2004, 41(14): 3707–3733
48. Xu F, Sun G, Li G, et al. Experimental study on crashworthiness of tailor-welded blank (TWB) thin walled high-strength steel (HSS) tubular structures. Thin-Walled Structures, 2014, 74: 12–27
49. Otubushin A. Detailed validation of a non-linear finite element code using dynamic axial crushing of a square tube. International Journal of Impact Engineering, 1998, 21(5): 349–368
50. Rusinek A, Zaera R, Forquin P, et al. Effect of plastic deformation and boundary conditions combined with elastic wave propagation on the collapse site of a crash box. Thin-Walled Structures, 2008, 46(10): 1143–1163
51. Gümrük R, Karadeniz S. A numerical study of the influence of bump type triggers on the axial crushing of top hat thin-walled sections. Thin-Walled Structures, 2008, 46(10): 1094–1106
52. Zhang X, Huh H. Energy absorption of longitudinally grooved square tubes under axial compression. Thin-Walled Structures, 2009, 47(12): 1469–1477
53. Langseth M, Hopperstad O. Static and dynamic axial crushing of square thin-walled aluminium extrusions. International Journal of Impact Engineering, 1996, 18(7–8): 949–968
54. Langseth M, Hopperstad O, Berstad T. Crashworthiness of aluminium extrusions: Validation of numerical simulation, effect of mass ratio and impact velocity. International Journal of Impact Engineering, 1999, 22(9–10): 829–854
55. Jensen Ø, Langseth M, Hopperstad O. Experimental investigations on the behavior of short to long square aluminium tubes subjected to axial loading. International Journal of Impact Engineering, 2004, 30(8–9): 973–1003
56. Stronge W, Yu T, Johnson W. Long stroke energy dissipation in splitting tubes. International Journal of Mechanical Sciences, 1983, 25(9–10): 637–647
57. Reyes A, Langseth M, Hopperstad O S. Square aluminium tubes subjected to oblique loading. International Journal of Impact Engineering, 2003, 28(10): 1077–1106
58. Nia A A, Fallah Nejad K, Badnava H, et al. Effects of buckling initiators on mechanical behavior of thin-walled square tubes subjected to oblique loading. Thin-Walled Structures, 2012, 59: 87–96
59. Zhang X, Cheng G, You Z, et al. Energy absorption of axially compressed thin-walled square tubes with patterns. Thin-Walled Structures, 2007, 45(9): 737–746
60. Arnold B, Altenhof W. Experimental observations on the crush characteristics of AA6061 T4 and T6 structural square tubes with and without circular discontinuities. International Journal of Crashworthiness, 2004, 9(1): 73–87
61. Cheng Q, Altenhof W, Li L. Experimental investigations on the crush behavior of AA6061-T6 aluminium square tubes with different types of through-hole discontinuities. Thin-Walled Structures, 2006, 44(4): 441–454
62. Zhang X, Zhang H. Crush resistance of square tubes with various thickness configurations. International Journal of Mechanical Sciences, 2016, 107: 58–68
63. Fyllingen Ø, Hopperstad O, Langseth M. Stochastic simulations of square aluminium tubes subjected to axial loading. International Journal of Impact Engineering, 2007, 34(10): 1619–1636
64. Mamalis A, Johnson W. The quasi-static crumpling of thin-walled circular cylinders and frusta under axial compression. International Journal of Mechanical Sciences, 1983, 25(9–10): 713–732
65. Mamalis A, Manolakos D, Saigal S, et al. Extensible plastic collapse of thin-wall frusta as energy absorbers. International Journal of Mechanical Sciences, 1986, 28(4): 219–229
66. Reid S, Reddy T. Static and dynamic crushing of tapered sheet metal tubes of rectangular cross-section. International Journal of Mechanical Sciences, 1986, 28(9): 623–637
67. Nagel G, Thambiratnam D. Computer simulation and energy absorption of tapered thin-walled rectangular tubes. Thin-Walled Structures, 2005, 43(8): 1225–1242
68. El-Sobky H, Singace A, Petsios M. Mode of collapse and energy absorption characteristics of constrained frusta under axial impact loading. International Journal of Mechanical Sciences, 2001, 43(3): 743–757
69. Alghamdi A, Aljawi A, Abu-Mansour T N. Modes of axial collapse of unconstrained capped frusta. International Journal of Mechanical Sciences, 2002, 44(6): 1145–1161
70. Alghamdi A. Folding-crumpling of thin-walled aluminium frusta. International Journal of Crashworthiness, 2002, 7(1): 67–78
71. Gupta N, Prasad G E, Gupta S. Plastic collapse of metallic conical frusta of large semi-apical angles. International Journal of Crashworthiness, 1997, 2(4): 349–366
72. Prasad G E, Gupta N. An experimental study of deformation

modes of domes and large-angled frusta at different rates of compression. International Journal of Impact Engineering, 2005, 32(1–4): 400–415
73. Niknejad A, Tavassolimanesh A. Axial compression of the empty capped-end frusta during the inversion progress. Materials & Design, 2013, 49: 65–75
74. Chahardoli S, Nia A A. Experimental and numerical investigations on collapse properties of capped-end frusta tubes with circular triggers under axial quasi-static loading. International Journal of Mechanical Sciences, 2017, 134: 545–561
75. Mamalis A, Johnson W, Viegelahn G. The crumpling of steel thin-walled tubes and frusta under axial compression at elevated strain-rates: Some experimental results. International Journal of Mechanical Sciences, 1984, 26(11–12): 537–547
76. Nagel G, Thambiratnam D. A numerical study on the impact response and energy absorption of tapered thin-walled tubes. International Journal of Mechanical Sciences, 2004, 46(2): 201–216
77. Nagel G, Thambiratnam D. Dynamic simulation and energy absorption of tapered tubes under impact loading. International Journal of Crashworthiness, 2004, 9(4): 389–399
78. Nagel G M, Thambiratnam D P. Dynamic simulation and energy absorption of tapered thin-walled tubes under oblique impact loading. International Journal of Impact Engineering, 2006, 32(10): 1595–1620
79. Taştan A, Acar E, Güler M, et al. Optimum crashworthiness design of tapered thin-walled tubes with lateral circular cutouts. Thin-Walled Structures, 2016, 107: 543–553
80. Mamalis A, Robinson M, Manolakos D, et al. Crashworthy capability of composite material structures. Composite Structures, 1997, 37(2): 109–134
81. Shin K C, Lee J J, Kim K H, et al. Axial crush and bending collapse of an aluminium/GFRP hybrid square tube and its energy absorption capability. Composite Structures, 2002, 57(1–4): 279–287
82. Ramakrishna S, Hull D. Energy absorption capability of epoxy composite tubes with knitted carbon fibre fabric reinforcement. Composites Science and Technology, 1993, 49(4): 349–356
83. Solaimurugan S, Velmurugan R. Influence of fibre orientation and stacking sequence on petalling of glass/polyester composite cylindrical shells under axial compression. International Journal of Solids and Structures, 2007, 44(21): 6999–7020
84. Kim J S, Yoon H J, Shin K B. A study on crushing behaviors of composite circular tubes with different reinforcing fibers. International Journal of Impact Engineering, 2011, 38(4): 198–207
85. Hamada H, Ramakrishna S, Satoh H. Crushing mechanism of carbon fibre/PEEK composite tubes. Composites, 1995, 26(11): 749–755
86. Song H W, Wan Z M, Xie Z M, et al. Axial impact behavior and energy absorption efficiency of composite wrapped metal tubes. International Journal of Impact Engineering, 2000, 24(4): 385–401
87. Mirzaei M, Shakeri M, Sadighi M, et al. Experimental and analytical assessment of axial crushing of circular hybrid tubes under quasi-static load. Composite Structures, 2012, 94(6): 1959–1966
88. Mahdi E, Sultan H, Hamouda A, et al. Experimental optimization of composite collapsible tubular energy absorber device. Thin-Walled Structures, 2006, 44(11): 1201–1211
89. Thuis H, Metz V. The influence of trigger configurations and laminate lay-up on the failure mode of composite crush cylinders. Composite Structures, 1994, 28(2): 131–137
90. Siromani D, Henderson G, Mikita D, et al. An experimental study on the effect of failure trigger mechanisms on the energy absorption capability of CFRP tubes under axial compression. Composites. Part A, Applied Science and Manufacturing, 2014, 64: 25–35
91. Huang J, Wang X. Numerical and experimental investigations on the axial crushing response of composite tubes. Composite Structures, 2009, 91(2): 222–228
92. Chiu L N, Falzon B G, Ruan D, et al. Crush responses of composite cylinder under quasi-static and dynamic loading. Composite Structures, 2015, 131: 90–98
93. Mahdi E, Mokhtar A, Asari N, et al. Nonlinear finite element analysis of axially crushed cotton fibre composite corrugated tubes. Composite Structures, 2006, 75(1–4): 39–48
94. Abdewi E F, Sulaiman S, Hamouda A, et al. Effect of geometry on the crushing behavior of laminated corrugated composite tubes. Journal of Materials Processing Technology, 2006, 172(3): 394–399
95. Abdewi E F, Sulaiman S, Hamouda A, et al. Quasi-static axial and lateral crushing of radial corrugated composite tubes. Thin-Walled Structures, 2008, 46(3): 320–332
96. Mamalis A, Manolakos D, Demosthenous G, et al. The static and dynamic axial crumbling of thin-walled fibreglass composite square tubes. Composites. Part B, Engineering, 1997, 28(4): 439–451
97. Mamalis A G, Manolakos D, Ioannidis M, et al. Crashworthy characteristics of axially statically compressed thin-walled square CFRP composite tubes: Experimental. Composite Structures, 2004, 63(3–4): 347–360
98. Mamalis A, Manolakos D, Ioannidis M, et al. On the experimental investigation of crash energy absorption in laminate splaying collapse mode of FRP tubular components. Composite Structures, 2005, 70(4): 413–429
99. Mamalis A, Manolakos D, Ioannidis M, et al. The static and dynamic axial collapse of CFRP square tubes: Finite element modelling. Composite Structures, 2006, 74(2): 213–225
100. Zarei H, Kröger M, Albertsen H. An experimental and numerical crashworthiness investigation of thermoplastic composite crash boxes. Composite Structures, 2008, 85(3): 245–257
101. Bambach M R, Elchalakani M, Zhao X L. Composite steel–CFRP SHS tubes under axial impact. Composite Structures, 2009, 87(3): 282–292
102. Bambach M R, Jama H H, Elchalakani M. Static and dynamic axial crushing of spot-welded thin-walled composite steel–CFRP square tubes. International Journal of Impact Engineering, 2009, 36(9): 1083–1094
103. Bambach M R, Elchalakani M. Plastic mechanism analysis of steel SHS strengthened with CFRP under large axial deformation. Thin-Walled Structures, 2007, 45(2): 159–170

104. Bambach M. Axial capacity and crushing behavior of metal–fiber square tubes–Steel, stainless steel and aluminium with CFRP. Composites. Part B, Engineering, 2010, 41(7): 550–559
105. Bambach M. Axial capacity and crushing of thin-walled metal, fibre–epoxy and composite metal–fibre tubes. Thin-Walled Structures, 2010, 48(6): 440–452
106. Zheng Z, Liu Y, Yu J, et al. Dynamic crushing of cellular materials: Continuum-based wave models for the transitional and shock modes. International Journal of Impact Engineering, 2012, 42: 66–79
107. Zheng Z, Yu J, Wang C, et al. Dynamic crushing of cellular materials: A unified framework of plastic shock wave models. International Journal of Impact Engineering, 2013, 53: 29–43
108. Liu Y, Schaedler T A, Chen X. Dynamic energy absorption characteristics of hollow microlattice structures. Mechanics of Materials, 2014, 77: 1–13
109. Reid S, Reddy T, Gray M. Static and dynamic axial crushing of foam-filled sheet metal tubes. International Journal of Mechanical Sciences, 1986, 28(5): 295–322
110. Reid S, Reddy T. Axial crushing of foam-filled tapered sheet metal tubes. International Journal of Mechanical Sciences, 1986, 28(10): 643–656
111. Reddy T, Wall R. Axial compression of foam-filled thin-walled circular tubes. International Journal of Impact Engineering, 1988, 7(2): 151–166
112. Seitzberger M, Rammerstorfer F G, Gradinger R, et al. Experimental studies on the quasi-static axial crushing of steel columns filled with aluminium foam. International Journal of Solids and Structures, 2000, 37(30): 4125–4147
113. Güden M, Kavi H. Quasi-static axial compression behavior of constraint hexagonal and square-packed empty and aluminium foam-filled aluminium multi-tubes. Thin-Walled Structures, 2006, 44(7): 739–750
114. Abramowicz W, Wierzbicki T. Axial crushing of foam-filled columns. International Journal of Mechanical Sciences, 1988, 30 (3–4): 263–271
115. Seitzberger M, Rammerstorfer F G, Degischer H P, et al. Crushing of axially compressed steel tubes filled with aluminium foam. Acta Mechanica, 1997, 125(1–4): 93–105
116. Guillow S, Lu G, Grzebieta R. Quasi-static axial compression of thin-walled circular aluminium tubes. International Journal of Mechanical Sciences, 2001, 43(9): 2103–2123
117. Hanssen A, Langseth M, Hopperstad O. Static crushing of square aluminium extrusions with aluminium foam filler. International Journal of Mechanical Sciences, 1999, 41(8): 967–993
118. Hanssen A G, Langseth M, Hopperstad O S. Static and dynamic crushing of square aluminium extrusions with aluminium foam filler. International Journal of Impact Engineering, 2000, 24(4): 347–383
119. Santosa S P, Wierzbicki T, Hanssen A G, et al. Experimental and numerical studies of foam-filled sections. International Journal of Impact Engineering, 2000, 24(5): 509–534
120. Kavi H, Toksoy A K, Guden M. Predicting energy absorption in a foam-filled thin-walled aluminium tube based on experimentally determined strengthening coefficient. Materials & Design, 2006, 27(4): 263–269
121. Mirfendereski L, Salimi M, Ziaei-Rad S. Parametric study and numerical analysis of empty and foam filled thin-walled tubes under static and dynamic loadings. International Journal of Mechanical Sciences, 2008, 50(6): 1042–1057
122. Ahmad Z, Thambiratnam D, Tan A. Dynamic energy absorption characteristics of foam-filled conical tubes under oblique impact loading. International Journal of Impact Engineering, 2010, 37(5): 475–488
123. Meguid S, Attia M, Monfort A. On the crush behavior of ultralight foam-filled structures. Materials & Design, 2004, 25(3): 183–189
124. Santosa S, Wierzbicki T. Crash behavior of box columns filled with aluminium honeycomb or foam. Computers & Structures, 1998, 68(4): 343–367
125. Zhang Z, Liu S, Tang Z. Comparisons of honeycomb sandwich and foam-filled cylindrical columns under axial crushing loads. Thin-Walled Structures, 2011, 49(9): 1071–1079
126. Yin H, Wen G, Hou S, et al. Crushing analysis and multiobjective crashworthiness optimization of honeycomb-filled single and bitubular polygonal tubes. Materials & Design, 2011, 32(8–9): 4449–4460
127. Hussein R D, Ruan D, Lu G, et al. Crushing response of square aluminium tubes filled with polyurethane foam and aluminium honeycomb. Thin-Walled Structures, 2017, 110: 140–154
128. Mamalis A, Manolakos D, Ioannidis M, et al. Finite element simulation of the axial collapse of metallic thin-walled tubes with octagonal cross-section. Thin-Walled Structures, 2003, 41(10): 891–900
129. Rossi A, Fawaz Z, Behdinan K. Numerical simulation of the axial collapse of thin-walled polygonal section tubes. Thin-Walled Structures, 2005, 43(10): 1646–1661
130. Zhang X, Huh H. Crushing analysis of polygonal columns and angle elements. International Journal of Impact Engineering, 2010, 37(4): 441–451
131. Zhang X, Cheng G, Zhang H. Theoretical prediction and numerical simulation of multi-cell square thin-walled structures. Thin-Walled Structures, 2006, 44(11): 1185–1191
132. Tran T, Hou S, Han X, et al. Theoretical prediction and crashworthiness optimization of multi-cell square tubes under oblique impact loading. International Journal of Mechanical Sciences, 2014, 89: 177–193
133. Tran T, Hou S, Han X, et al. Theoretical prediction and crashworthiness optimization of multi-cell triangular tubes. Thin-Walled Structures, 2014, 82: 183–195
134. Zheng G, Pang T, Sun G, et al. Theoretical, numerical, and experimental study on laterally variable thickness (LVT) multi-cell tubes for crashworthiness. International Journal of Mechanical Sciences, 2016, 118: 283–297
135. Zhang X, Zhang H. Energy absorption of multi-cell stub columns under axial compression. Thin-Walled Structures, 2013, 68: 156–163
136. Tang Z, Liu S, Zhang Z. Analysis of energy absorption characteristics of cylindrical multi-cell columns. Thin-Walled Structures, 2013, 62: 75–84
137. Yin H, Wen G, Liu Z, et al. Crashworthiness optimization design for foam-filled multi-cell thin walled structures. Thin-Walled Structures, 2014, 75: 8–17

138. Hong W, Fan H, Xia Z, et al. Axial crushing behaviors of multi-cell tubes with triangular lattices. International Journal of Impact Engineering, 2014, 63: 106–117
139. Tabacu S. Analysis of circular tubes with rectangular multi-cell insert under oblique impact loads. Thin-Walled Structures, 2016, 106: 129–147
140. Chirwa E. Theoretical analysis of tapered thin-walled metal inverbucktube. International Journal of Mechanical Sciences, 1993, 35(3–4): 325–351
141. Li G, Zhang Z, Sun G, et al. Comparison of functionally-graded structures under multiple loading angles. Thin-Walled Structures, 2015, 94: 334–347
142. Zhang X, Zhang H, Wen Z. Axial crushing of tapered circular tubes with graded thickness. International Journal of Mechanical Sciences, 2015, 92: 12–23
143. Li G, Xu F, Sun G, et al. A comparative study on thin-walled structures with functionally graded thickness (FGT) and tapered tubes withstanding oblique impact loading. International Journal of Impact Engineering, 2015, 77: 68–83
144. Zhang X, Wen Z, Zhang H. Axial crushing and optimal design of square tubes with graded thickness. Thin-Walled Structures, 2014, 84: 263–274
145. An X, Gao Y, Fang J, et al. Crashworthiness design for foam-filled thin-walled structures with functionally lateral graded thickness sheets. Thin-Walled Structures, 2015, 91: 63–71
146. Gupta P. A study on mode of collapse of varying wall thickness metallic frusta subjected to axial compression. Thin-Walled Structures, 2008, 46(5): 561–571
147. Zhang X, Zhang H. Relative merits of conical tubes with graded thickness subjected to oblique impact loads. International Journal of Mechanical Sciences, 2015, 98: 111–125
148. Zhang H, Zhang X. Crashworthiness performance of conical tubes with nonlinear thickness distribution. Thin-Walled Structures, 2016, 99: 35–44
149. Fang J, Gao Y, Sun G, et al. Dynamic crashing behavior of new extrudable multi-cell tubes with a functionally graded thickness. International Journal of Mechanical Sciences, 2015, 103: 63–73
150. Sun G, Xu F, Li G, et al. Crashing analysis and multiobjective optimization for thin-walled structures with functionally graded thickness. International Journal of Impact Engineering, 2014, 64: 62–74
151. Haghi Kashani M, Shahsavari Alavijeh H, Akbarshahi H, et al. Bitubular square tubes with different arrangements under quasi-static axial compression loading. Materials & Design, 2013, 51: 1095–1103
152. Sharifi S, Shakeri M, Fakhari H E, et al. Experimental investigation of bitubal circular energy absorbers under quasi-static axial load. Thin-Walled Structures, 2015, 89: 42–53
153. Goel M D. Deformation, energy absorption and crushing behavior of single-, double- and multi-wall foam filled square and circular tubes. Thin-Walled Structures, 2015, 90: 1–11
154. Azimi M B, Asgari M. A new bi-tubular conical–circular structure for improving crushing behavior under axial and oblique impacts. International Journal of Mechanical Sciences, 2016, 105: 253–265
155. Nia A A, Chahardoli S. Mechanical behavior of nested multi-tubular structures under quasi-static axial load. Thin-Walled Structures, 2016, 106: 376–389
156. Estrada Q, Szwedowicz D, Rodriguez-Mendez A, et al. Effect of radial clearance and holes as crush initiators on the crashworthiness performance of bi-tubular profiles. Thin-Walled Structures, 2019, 140: 43–59
157. Sun F, Lai C, Fan H, et al. Crushing mechanism of hierarchical lattice structure. Mechanics of Materials, 2016, 97: 164–183
158. Sun F, Lai C, Fan H. In-plane compression behavior and energy absorption of hierarchical triangular lattice structures. Materials & Design, 2016, 100: 280–290
159. Luo Y, Fan H. Energy absorbing ability of rectangular self-similar multi-cell sandwich-walled tubular structures. Thin-Walled Structures, 2018, 124: 88–97
160. Li W, Luo Y, Li M, et al. A more weight-efficient hierarchical hexagonal multi-cell tubular absorber. International Journal of Mechanical Sciences, 2018, 140: 241–249
161. Fan H, Luo Y, Yang F, et al. Approaching perfect energy absorption through structural hierarchy. International Journal of Engineering Science, 2018, 130: 12–32
162. Chen Y, Qiao C, Qiu X, et al. A novel self-locked energy absorbing system. Journal of the Mechanics and Physics of Solids, 2016, 87: 130–149
163. Yang K, Qin Q, Zhai Z, et al. Dynamic response of self-locked energy absorption system under impact loadings. International Journal of Impact Engineering, 2018, 122: 209–227
164. Yang K, Chen Y, Zhang L, et al. Shape and geometry design for self-locked energy absorption systems. International Journal of Mechanical Sciences, 2019, 156: 312–328
165. Baroutaji A, Gilchrist M, Olabi A G J T W S. Quasi-static, impact and energy absorption of internally nested tubes subjected to lateral loading. Thin-Walled Structures, 2016, 98: 337–350
166. Olabi A G, Morris E, Hashmi M, et al. Optimised design of nested oblong tube energy absorbers under lateral impact loading. International Journal of Impact Engineering, 2008, 35(1): 10–26
167. Olabi A G, Morris E, Hashmi M, et al. Optimised design of nested circular tube energy absorbers under lateral impact loading. International Journal of Mechanical Sciences, 2008, 50(1): 104–116
168. Wang H, Yang J, Liu H, et al. Internally nested circular tube system subjected to lateral impact loading. Thin-Walled Structures, 2015, 91: 72–81
169. Tarlochan F, Ramesh S. Composite sandwich structures with nested inserts for energy absorption application. Composite Structures, 2012, 94(3): 904–916
170. Reddy T, Reid S. Axial splitting of circular metal tubes. International Journal of Mechanical Sciences, 1986, 28(2): 111–131
171. Zhang X, Yu T. Energy absorption of pressurized thin-walled circular tubes under axial crushing. International Journal of Mechanical Sciences, 2009, 51(5): 335–349
172. Chen W, Wierzbicki T. Relative merits of single-cell, multi-cell and foam-filled thin-walled structures in energy absorption. Thin-Walled Structures, 2001, 39(4): 287–306
173. Ahmad Z, Thambiratnam D. Crushing response of foam-filled

conical tubes under quasi-static axial loading. Materials & Design, 2009, 30(7): 2393–2403

174. Alavi Nia A, Haddad Hamedani J. Comparative analysis of energy absorption and deformations of thin walled tubes with various section geometries. Thin-Walled Structures, 2010, 48(12): 946–954

175. Zhang X, Cheng G. A comparative study of energy absorption characteristics of foam-filled and multicell square columns. International Journal of Impact Engineering, 2007, 34(11): 1739–1752